Stem Cell Reports
Article

OPEN ACCESS

Evaluating Synthetic Activation and Repression of Neuropsychiatric-Related Genes in hiPSC-Derived NPCs, Neurons, and Astrocytes

Seok-Man Ho,[1,3,5,8] Brigham J. Hartley,[1,5,8] Erin Flaherty,[2,5] Prashanth Rajarajan,[2,5] Rawan Abdelaal,[6,7] Ifeanyi Obiorah,[1,5] Natalie Barretto,[1,2,5] Hamza Muhammad,[1,2,5] Hemali P. Phatnani,[6,7] Schahram Akbarian,[1,2,5] and Kristen J. Brennand[1,2,4,5,*]

[1]Department of Psychiatry
[2]Department of Neuroscience
[3]Department of Cell, Developmental and Regenerative Biology
[4]Department of Genetics and Genomics
[5]Friedman Brain Institute
Icahn School of Medicine at Mount Sinai, New York, NY 10029, USA
[6]Center for Genomics of Neurodegenerative Disease, New York Genome Center, New York, NY 10013, USA
[7]Department of Biochemistry and Molecular Biophysics, Columbia University Medical Center, New York, NY 10032, USA
[8]Co-first author
*Correspondence: kristen.brennand@mssm.edu
http://dx.doi.org/10.1016/j.stemcr.2017.06.012

SUMMARY

Modulation of transcription, either synthetic activation or repression, via dCas9-fusion proteins is a relatively new methodology with the potential to facilitate high-throughput up- or downregulation studies of gene function. Genetic studies of neurodevelopmental disorders have identified a growing list of risk variants, including both common single-nucleotide variants and rare copy-number variations, many of which are associated with genes having limited functional annotations. By applying a CRISPR-mediated gene-activation/repression platform to populations of human-induced pluripotent stem cell-derived neural progenitor cells, neurons, and astrocytes, we demonstrate that it is possible to manipulate endogenous expression levels of candidate neuropsychiatric risk genes across these three cell types. Although proof-of-concept studies using catalytically inactive Cas9-fusion proteins to modulate transcription have been reported, here we present a detailed survey of the reproducibility of gRNA positional effects across a variety of neurodevelopmental disorder-relevant risk genes, donors, neural cell types, and dCas9 effectors.

INTRODUCTION

Risk variants for neurodevelopmental disorders such as schizophrenia (SZ) include both common single-nucleotide variants (SNVs) with small effects sizes (Schizophrenia Working Group of the Psychiatric Genomics Consortium, 2014) and copy-number variations (CNVs) with greater penetrance (CNV and Schizophrenia Working Groups of the Psychiatric Genomics Consortium; Psychosis Endophenotypes International Consortium, 2017). The majority of SZ-associated SNVs reside in genomic loci outside of coding regions (Schizophrenia Working Group of the Psychiatric Genomics Consortium, 2014), and may function as *cis*-acting expression quantitative trait loci (*cis*-eQTLs) (Fromer et al., 2016); however, they are frequently associated with genes that have limited functional annotation, making the connection between gene function and disease risk difficult to untangle. Moreover, because SZ-associated CNVs are large structural deletions or duplications of genomic sequence that generally encompass multiple genes (CNV and Schizophrenia Working Groups of the Psychiatric Genomics Consortium; Psychosis Endophenotypes International Consortium, 2017), defining the gene(s) responsible for disease risk can be difficult to resolve.

Designing reverse genetic experiments to ascertain the function of SZ-associated genes is hampered by the paucity of (and inability to manipulate) postmortem tissue from SZ patients. Human-induced pluripotent stem cell (hiPSC)-derived neural cells represent a novel strategy by which to model the genes underlying SZ predisposition. Using hiPSC-derived neural cells, we have previously demonstrated aberrant gene expression, protein levels and migration in SZ hiPSC-derived neural progenitor cells (NPCs) (Brennand et al., 2015; Topol et al., 2015, 2016), and diminished neuronal connectivity and synaptic activity in SZ hiPSC-derived neurons (Brennand et al., 2011; Yu et al., 2014). Although these hiPSC-based studies partially reflect postmortem pathological (Wong and Van Tol, 2003) and SZ-rodent model (well-reviewed by Jaaro-Peled et al., 2010) findings, the precise functional dissection of SZ "risk genes" in hiPSC neuronal models has been challenging, except for small studies of rare families with SZ-associated inherited mutations (Lin et al., 2016; Srikanth et al., 2015; Wen et al., 2014; Yoon et al., 2014; Zhao et al., 2015). The ability to precisely modulate SZ disease-relevant gene expression in hiPSC-derived neural cell types would allow hiPSC models to better define the contribution and function of more genes associated with SZ disease risk.

The bacterial type II clustered regularly interspaced short palindromic repeat (CRISPR) and CRISPR-associated (Cas) protein system of *Streptococcus pyogenes* evolved as a component of the prokaryotic immune system (Jinek et al., 2012) and has recently been repurposed for editing of the human genome (Cong et al., 2013). When complexed with an artificial single guide RNA (gRNA) to form an RNA-guided endonuclease, Cas9 can be directed to almost any genomic location, provided that the 20 base pair nucleotide gRNA target sequence satisfies the protospacer-adjacent motif requirement (Cong et al., 2013). Such limited target sequence requirements, together with the simplicity and ease of cloning synthesized gRNAs, has led to novel applications beyond genome editing. By simultaneously introducing nuclease-null mutations into Cas9 (Gilbert et al., 2013; Qi et al., 2013), and coupling the catalytically inactive or dead Cas9 (dCas9) to a variety of effector protein domains, the modulation of transcription (Gilbert et al., 2013; Qi et al., 2013), DNA methylation (McDonald et al., 2016; Vojta et al., 2016), and histone modifications (Hilton et al., 2015) have all been demonstrated. Activation or repression of transcription using dCas9-fusion protein variants represents a novel methodology to design gain- or loss-of-function studies with high fidelity. As this modulation occurs at the endogenous level, it is predicted to include the full range of alternative splice isoforms, which are frequently overlooked by RNAi technologies or the use of cDNA overexpression approaches. While a growing number of proof-of-concept studies have demonstrated the successful application of a variety of dCas9-fusion proteins to the up- and downregulation of endogenous expression, few, if any, have systematically described the inter-gene, inter-individual, inter-cell type, and inter-effector variation in the practical application of this system.

Using hiPSC-derived neural cells, we set out to systemically test the ability of different gRNAs targeting the presumptive promoter regions of five different SZ-associated risk genes: potassium channel tetramerization domain containing 13 (*KCTD13*) and thousand and one amino acid protein kinase 2 (*TOAK2*) resides within 16p11.2, and neurexin 1 (*NRXN1*) within 2p16.3, two loci where recurrent CNVs are associated with intellectual disability, autism spectrum disorder, SZ, and other neuropsychiatric disorders (CNV and Schizophrenia Working Groups of the Psychiatric Genomics Consortium; Psychosis Endophenotypes International Consortium, 2017; Maillard et al., 2015), whereas synaptosome-associated protein 91 (*SNAP91*) and chloride voltage-gated channel 3 (*CLCN3*) have both recently been implicated with SZ risk via *cis*-eQTLs genome-wide association study variant analysis (Fromer et al., 2016). By evaluating dCas9-mediated transcriptional modulation using three different platforms (downregulation using a dCas9 fusion to the Krüppel-associated box [KRAB] repressor domain [Thakore et al., 2015]; upregulation using a dCas9 fusion to the tetrameric VP16 transcription activator domain [VP64] [Kearns et al., 2014; Maeder et al., 2013] or the tripartite activator, VP64-p65-Rta (VPR) [Chavez et al., 2015, 2016]), in three different hiPSC-derived neural cell types (NPCs, neurons, and astrocytes) (Figure 1), using hiPSCs reprogrammed from three unique donors (Table S1), we describe the efficacy and variability of dCas9-protein fusion-based transcriptional modulation in hiPSC-based studies.

RESULTS

Gene expression profiling indicates that our hiPSC NPCs most resemble cells in the fetal cortical and subcortical forebrain regions (Brennand et al., 2015). NPCs are a replicative population of SOX2-positive and NESTIN-positive cells with the capacity to differentiate to populations comprised of ~80% neurons (predominantly excitatory) and ~20% astrocytes (Brennand et al., 2011). Lentiviral transduction of NPCs with doxycycline-inducible human *NGN2* rapidly yields excitatory neurons with robust electrical activity and detectable synaptic puncta within 3 weeks (Ho et al., 2016); they can also be differentiated to a population of hiPSC-astrocytes that shares the transcriptional profile and functional characteristics of human fetal astrocytes via a 30-day protocol (TCW et al., 2017). qPCR characterization of hiPSC-derived NPCs, neurons, *NGN2* neurons, and astrocytes demonstrated baseline expression of all five SZ-risk genes considered herein, *KCTD13, TOAK2, NRXN1, SNAP91,* and *CLCN3* (Figure S1), prior to dCas9-manipulation.

The Efficacy of dCas9-Mediated Transcript Activation Varies Extensively between Genes and Is Not Necessarily Consistent between Unique Donors

A variety of human genes (*VEGFA, NTF3* [Maeder et al., 2013], *SOX2* [Kearns et al., 2014], and *ASCL1, NEUROD1, MIAT1,* and *RHOFX2* [Chavez et al., 2015, 2016]) have now been activated using dCas9 effectors in HEK293T cells or hiPSCs, although the extent to which any given gene is amenable to upregulation across a larger number of cell types is unclear; here we applied two well-established dCas9 transcriptional activators, dCas9^{-VP64} and dCas9^{-VPR}, to hiPSC-derived NPCs and neurons (Figures 1A and 1B). As extensive transcriptional variability exists between hiPSCs from different donors (Carcamo-Orive et al., 2017; Nishizawa et al., 2016; Rouhani et al., 2014), we first considered how well the activating capabilities of both platforms translated across five genes (Figure 1C) using neural cells from three unique donors. For each gene,

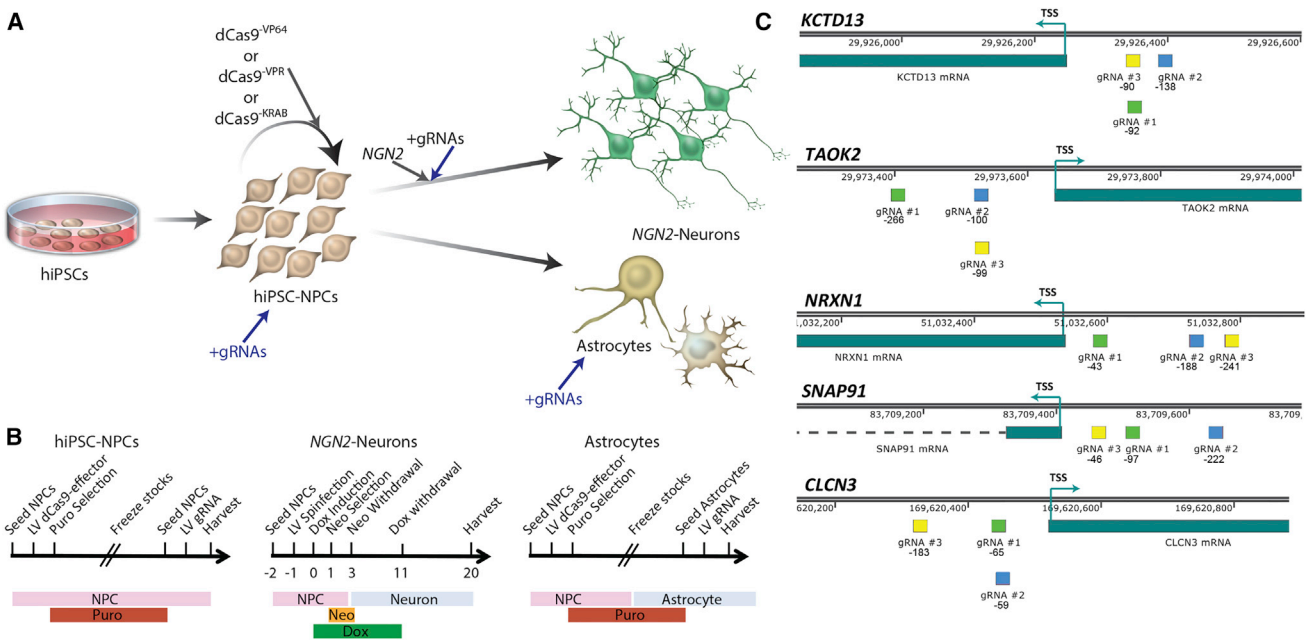

Figure 1. Experimental Platform to Evaluate dCas9-Mediated Manipulation of Gene Expression in hiPSC-Derived NPCs, Neurons, and Astrocytes

(A) Experimental schematic for the generation of hiPSC-derived NPCs, neurons, and astrocytes, including the administration of lentiviral dCas9 and gRNA vectors.

(B) Experimental time line for lentiviral transduction (and antibiotic selection) of hiPSC-derived NPCs, neurons, and astrocytes with lentiviral dCas9 and gRNA vectors.

(C) gRNA locations (green, blue, and yellow) relative to the TSS of *KCTD13*, *TAOK2*, *NRXN1*, *SNAP91*, and *CLCN3*.

gRNAs were designed to target at least three distinct locations upstream of the transcriptional start site (TSS), and thus within the putative promoter elements (Figure 1C; Table S2). Both antibiotic-selected (Figure S2) and non-selected lentiviral-transduced dCas9^{-VP64} and dCas9^{-VPR} NPCs were evaluated.

First, transcriptional modulation of *KCTD13* and *TOAK2* was evaluated in NPCs. Across hiPSC-NPC lines from three unique donors, following the transduction of different lentiviruses encoding three distinct gRNAs, two *KCTD13* gRNAs (2 and 3) significantly increased *KCTD13* in dCas9^{-VP64} NPCs from two of the three individuals tested (gRNA 2: C1, 2.22-fold, $p \leq 0.01$; C2, 1.87-fold, $p \leq 0.01$; n = 3 each; gRNA 3: C1, 1.85-fold, $p \leq 0.05$; C2, 1.48-fold, $p \leq 0.05$; n = 3 each; antibiotic selection for dCas9^{-VP64}) (Figure 2A). Activation of *TOAK2* by gRNAs targeted to three different locations upstream of the TSS failed to increase expression in dCas9^{-VP64} NPCs across both individuals tested (antibiotic selection for dCas9^{-VP64}) (Figure 2B).

Second, across six gRNAs generated to the promoter regions to *NRXN1*, we failed to observe robust increases in expression with either dCas9^{-VP64} or dCas9^{-VPR} NPCs (Figures 2C and S3), only achieving increased *NRXN1* expression in one individual with one gRNA using either the dCas9^{-VP64} and dCas9^{-VPR} effectors (gRNA 2: dCas9^{-VP64} C3, 5.66-fold, $p \leq 0.0001$; dCas9^{-VPR} C3, 8.53-fold, $p \leq 0.05$; n = 3 each; antibiotic selection for dCas9^{-VP64} and dCas9^{-VPR}) (Figure 2C). Three additional gRNAs, designed upstream of a second TSS, were also unable to increase *NRXN1* expression, with or without selection for dCas9^{-VP64} in one individual (Figure S3), demonstrating that testing up to six gRNAs does not ensure successful gene activation.

Third, highly expressed in neurons (Zhang et al., 2016), *SNAP91* and *CLCN3* transcriptional modulation was tested in *NEUROGENIN2* (*NGN2*)-induced populations of excitatory neurons (Ho et al., 2016; Zhang et al., 2013) after 8 days of maturation. Following transduction of three distinct gRNAs to *SNAP91*, in parallel with a lentivirus containing inducible *NGN2*, we found that gRNA 2 significantly increased *SNAP91* levels in dCas9^{-VPR} day 8 *NGN2* neurons from all three donors (gRNA 2: C1, 1.33-fold, $p \leq 0.01$; C2, 1.66-fold, $p \leq 0.01$; C3, 2.02-fold, $p \leq 0.001$; n = 3 each; no antibiotic selection for dCas9^{-VPR}) (Figure 2D), results that were confirmed by western blot for gRNA 2 (n = 1, antibiotic selection for dCas9^{-VPR}) (Figure S4A). *SNAP91* gRNA 2 also produced robust increases in

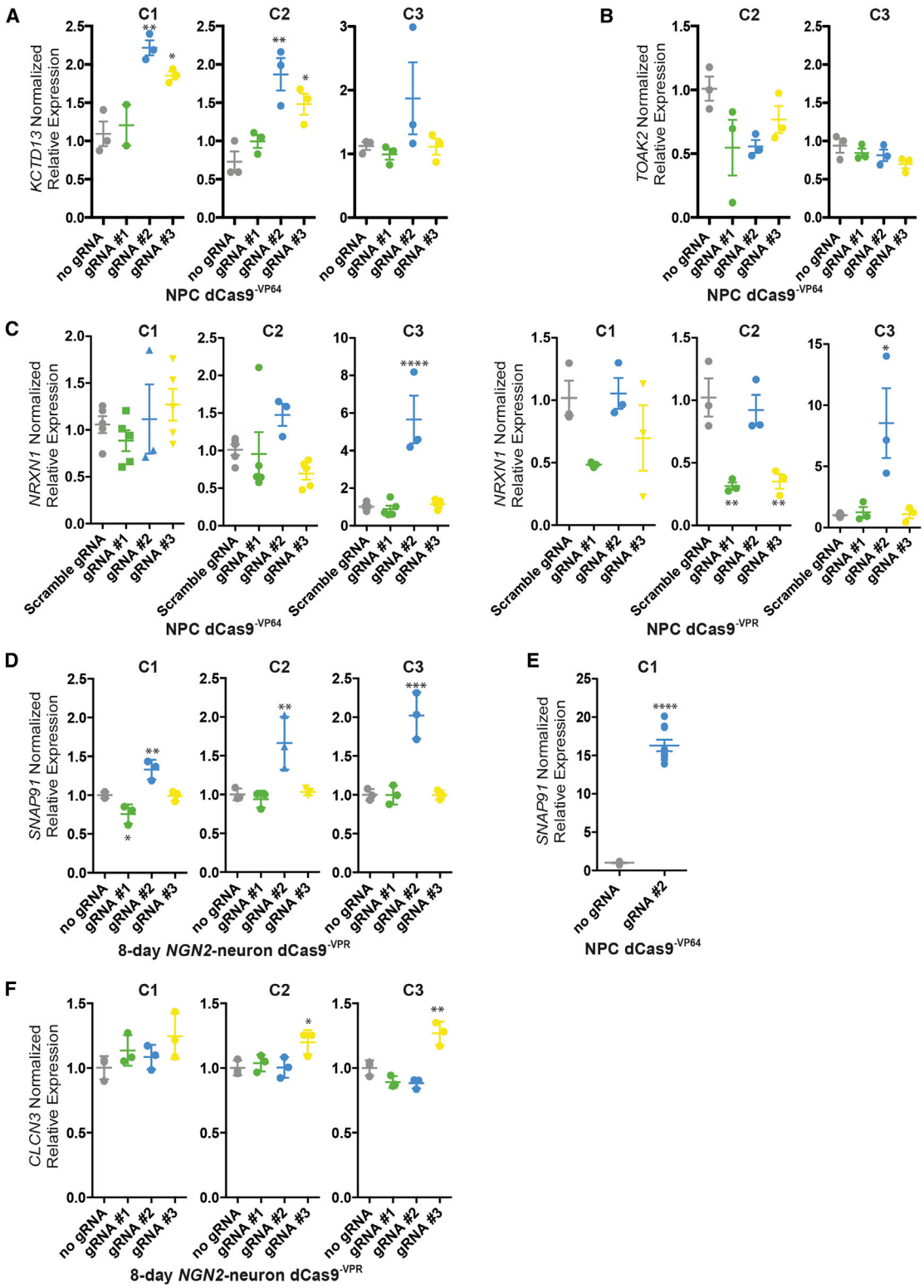

Figure 2. Activation of Neuropsychiatric Disorder Risk Genes in hiPSC-Derived NPCs and *NGN2* Neurons from Three Individuals

(A–F) Normalized relative mRNA levels (compared with no gRNA or scrambled gRNA control as indicated [gray]) following transduction of dCas9^{VP64} (A, B, C, and E) and dCas9^{VPR} (C, D, and F) in NPCs (A, B, C, and E) and 8-day-old *NGN2* neurons (D and F) with

(legend continued on next page)

SNAP91 levels in NPCs (C1, 16.31-fold, $p < 0.0001$; n = 9 each; antibiotic selection for dCas9^{-VPR}) (Figure 2E). Of the three *CLCN3* gRNAs evaluated, only gRNA 3 increased expression in dCas9^{-VPR} NPCs (C2, 1.20-fold, $p \leq 0.05$; C3, 1.27-fold, $p \leq 0.01$; n = 3 each; no antibiotic selection for dCas9^{-VPR}) (Figure 2F).

Altogether, these results demonstrate that designing three gRNAs is not necessarily sufficient to ensure successful manipulation of gene expression. Moreover, results are not always consistent across hiPSC-NPC lines derived from unique individuals. This variation could not be explained by differences in the levels of dCas9-effector protein (Figure S2A) or transcript (Figures S2B and S2C) between individuals. Therefore, we recommend validating gRNA efficacy across each individual hiPSC line to be evaluated.

Activating gRNAs Should Be Re-validated for dCas9^{-KRAB} Repression

A key question is whether a gRNA position capable of activating transcript expression via dCas9^{-VP64} or dCas9^{-VPR} will also reliably repress transcription for the same gene via dCas9^{-KRAB}. If true, this would reduce the necessary design, synthesis, cloning, and validation of different gRNAs for each experiment, facilitating more scalable experimental execution. We used the same gRNA positions examined in the activation setting (Figure 2), but in NPCs and neurons expressing dCas9^{-KRAB} fusion proteins (Figure 3). Again, both antibiotic-selected (Figure S2) and non-selected lentiviral-transduced dCas9^{-KRAB} NPCs were evaluated. Overall, gRNA efficacies with dCas9^{-KRAB} (Figure 3) were only sometimes consistent with those achieved for dCas9^{-VP64} or dCas9^{-VPR} (Figure 2).

Whereas *KCTD13* gRNA 2 and 3 were efficacious in dCas9^{-VP64} NPC lines from two individuals (Figure 2A), no gRNAs produced significant effects in dCas9^{-KRAB} NPCs (using the stringent multiple comparison statistical analysis used throughout; antibiotic selection for dCas9^{-KRAB}) (Figure 3A). Consistent with null effects observed in dCas9^{-VP64} NPCs (Figure 2B), none of the *TOAK2* gRNAs modulated transcription in dCas9^{-KRAB} NPCs (antibiotic selection for dCas9^{-KRAB}) (Figure 3B).

gRNA positional efficacy for activation (Figure 2) and repression (Figure 3) was somewhat consistent with *SNAP91* (gRNA 2 > gRNA 3/1) and *CLCN3* (gRNA 3 > gRNA 1/2). Similar to results with dCas9^{-VPR}, we found that *SNAP91* gRNA 2 had the most profound repressing effect in day 8 *NGN2* neuron populations (gRNA 2: C1, 0.43-fold, $p < 0.0001$; C2, 0.31-fold, $p < 0.0001$; C3, 0.24-fold, $p < 0.0001$; n = 3 each; no antibiotic selection for dCas9^{-KRAB}) (Figure 3C). *SNAP91* gRNA 2 also robustly decreased *SNAP91* levels in day 20 *NGN2* neurons (C1, 0.77-fold, $p < 0.001$; n = 9 each; antibiotic selection for dCas9^{-KRAB}) (Figure 3D). Surprisingly, when these same three gRNAs were tested in NPCs (rather than *NGN2* neurons) from these same three individuals, gRNA 3 rather than gRNA 2, showed greatest efficacy (C1, gRNA 2; 0.45-fold, $p < 0.0001$/gRNA 3; 0.29-fold, $p < 0.0001$; C2, gRNA 2; 0.46-fold, $p < 0.0001$/gRNA 3; 0.28-fold, $p < 0.0001$; C3, gRNA 2; 0.33-fold, $p < 0.0001$/gRNA 3; 0.19-fold, $p < 0.0001$; n = 3 each; antibiotic selection for dCas9^{-KRAB}) (Figure 3E). Efficacy of gRNA 2 in decreasing SNAP91 protein levels was confirmed by western blot (n = 3; antibiotic selection for dCas9^{-KRAB}) (Figure S4B). Although gRNAs against *CLCN3* were generally less efficacious, gRNA 3 produced significant effects (gRNA 3: C1, 0.85-fold, $p < 0.01$; C2, 0.74-fold, $p < 0.01$; C3, 0.82-fold, $p < 0.01$; n = 3 each; no antibiotic selection for dCas9^{-KRAB}) in day 8 *NGN2* neuron populations from all three NPC lines tested (Figure 3F).

Overall, these results demonstrate that gRNAs designed upstream of the TSS and validated for dCas9^{-VP64} or dCas9^{-VPR} should not be assumed to be effective when combined with dCas9^{-KRAB}. As observed with gene activation, dCas9^{-KRAB} results are not always consistent across unique individuals. Again, this variation could not be explained by differences in the levels of dCas9-effector protein (Figure S2A) or transcript (Figures S2B and S2C) between individuals. Surprisingly, in at least one case, gRNA efficacy in NPCs did not predict efficacy in neurons. We recommend validating gRNA efficacy across not just each individual hiPSC line to be evaluated, but also each dCas9 effector to be employed.

dCas9^{-VP64} Transcript Induction Efficacies Are Not Necessarily Consistent between NPCs, Neurons, Astrocytes, and HEK293T Cells

Given that chromatin states, particularly nucleosome positioning, can differ between cell types (Jiang and Pugh, 2009) and that nucleosomes can impede Cas9 access to DNA (Horlbeck et al., 2016b; Isaac et al., 2016), we next set out to determine whether gRNA activity in NPCs or neurons is predictive of efficacy in astrocytes. We differentiated astrocytes (NPC-astrocytes) (TCW et al., 2017; Xu et al., 2016) (Figure 4A) from the antibiotic-selected dCas9^{-VP64} NPC lines. NPC-astrocytes are positive for the astrocyte markers S100β, GFAP, and EAAT1 (Figures 4A

lentivirus-expressing gRNAs targeted to three different locations (green, blue, and yellow) upstream of the TSS for *KCTD13* (A), *TAOK2* (B), *NRXN1* (C), *SNAP91* (D and E), and *CLCN3* (F). C1–C3 indicates hiPSC lines from three independent male controls (see Table S1 for more information); each biological replicate is depicted by a circle.

Data are presented as means ± SEM (bar graph) from at least three independent biological replicates. *$p < 0.05$, **$p < 0.01$, ***$p < 0.001$, ****$p < 0.0001$.

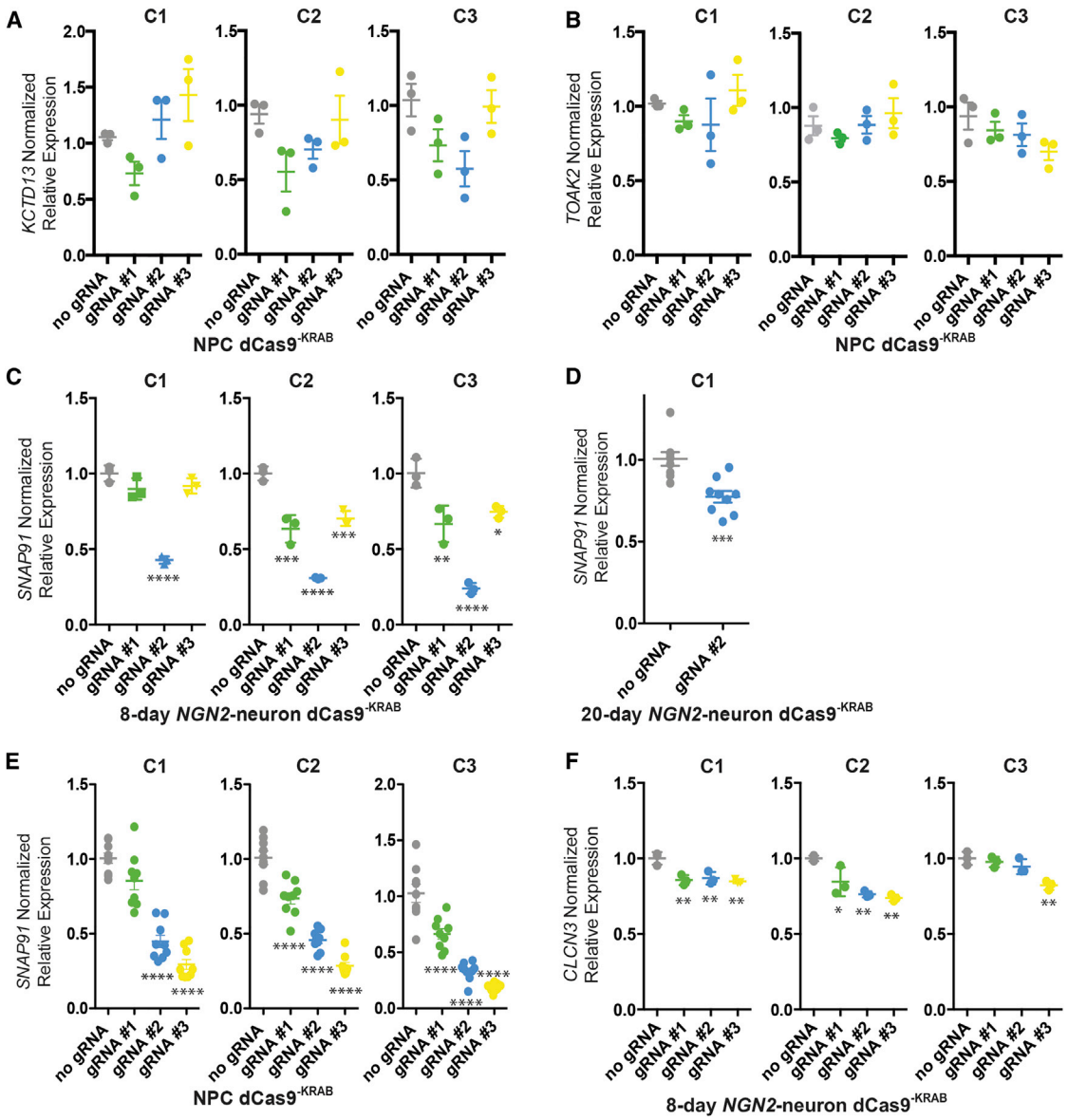

Figure 3. Repression of Neuropsychiatric Disorder Risk Genes in hiPSC-Derived NPCs and *NGN2* Neurons from Three Individuals

(A–F) Normalized relative mRNA levels (compared with no gRNA control [gray]) following transduction of dCas9^{KRAB} NPCs (A, B, and E), 8-day-old (C and F), and 20-day-old (D) *NGN2* neurons with lentivirus-expressing gRNAs targeted to different locations (green, blue, and yellow) upstream of the TSS for *KCTD13* (A), *TAOK2* (B), *SNAP91* (C, D, and E), and *CLCN3* (F). C1–C3 indicates hiPSC lines from three independent male controls (see Table S1 for more information); each biological replicate is depicted by a circle.

Data are presented as means ± SEM (bar graph) from at least three independent biological replicates. *p < 0.05, **p < 0.01, ***p < 0.001, ****p < 0.0001.

and 4B), and up to 90% of antibiotic-selected NPC-astrocytes were positive for dCas9 protein by fluorescence-activated cell sorting (FACS) (Figure 4C).

Transcriptional activation in dCas9^{-VP64} NPC-astrocytes (Figures 4D and 4E) was inconsistent with results observed in dCas9^{-VP64} NPCs and neurons (Figures 2A, 2D, and 2E). For *KCTD13*, only gRNA 2, and only in one individual, increased expression (C2, 1.28-fold, $p < 0.05$; n = 3; antibiotic selection for dCas9^{-VP64}). Unexpectedly, NPC-astrocytes were surprisingly more amenable to transcriptional activation of *SNAP91* (Figure 4E) than NPCs or neurons (Figures 2D, 2E, and 2F). *SNAP91* gRNAs 2 and 3 produced dramatic increases in expression in NPC-astrocytes, two orders of magnitude larger than those observed in NPC or

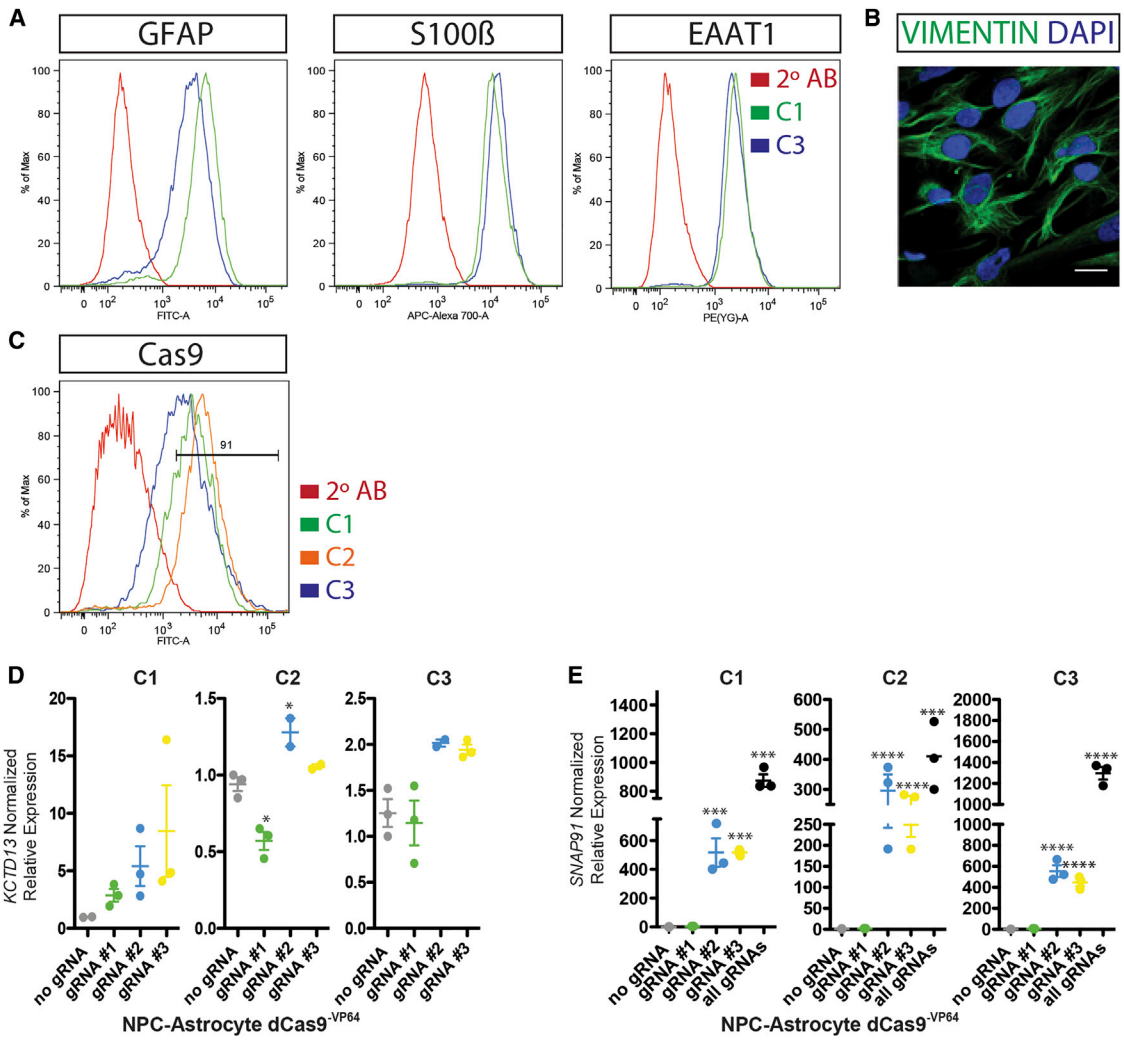

Figure 4. Activation of Neuropsychiatric Disorder Risk Genes in NPC-Derived Astrocytes from Three Individuals

(A) Representative FACS validation of NPC-astrocytes, using antibodies for GFAP (left), S100β (middle), and EAAT1 (right).

(B) Representative immunofluorescent image of NPC-astrocytes stained with vimentin (green) and DAPI (blue). Scale bar, 20 μm.

(C) FACS validation of Cas9 protein levels in dCas9^{-VP64} NPC-astrocytes.

(D and E) Normalized relative mRNA levels (compared with no gRNA control [gray]) following transduction of dCas9^{VP64} NPC-astrocytes with lentivirus-expressing gRNAs targeted to three different locations (green, blue, and yellow) upstream of the TSS for *KCTD13* (D) and *SNAP91* (E). C1–C3 indicates hiPSC lines from three independent male controls (see Table S1 for more information); each biological replicate is depicted by a circle.

Data are presented as means ± SEM (bar graph) from at least three independent biological replicates. *p < 0.05, ***p < 0.001, ****p < 0.0001.

neurons (C1, gRNA 2; 458.5-fold, p < 0.0001/gRNA 3; 405.5-fold, p < 0.0001; C2, gRNA 2; 248.4-fold, p < 0.0001/gRNA 3; 198.4-fold, p < 0.0001; C3, gRNA 2; 564.7-fold, p < 0.0001/gRNA 3; 467.7-fold, p < 0.0001; n = 3 each; antibiotic selection for dCas9^{-VP64}) (Figure 4E). Multiplexing of *SNAP91* gRNAs 1, 2, and 3 achieved greater efficacy than any single gRNA alone (Figure 4E).

There was surprisingly little correlation between gRNA efficacy in neural cells and HEK293T cells. While *KCTD13* gRNAs 2 and 3 proved efficacious in some (but not all) control dCas9^{VP64} NPCs, it was gRNAs 1 and 3 that increased expression in antibiotic-selected, but not unselected, dCas9^{-VP64} HEK293Ts (Figure S5A). Although *TOAK2* gRNAs failed to increase expression in dCas9^{VP64} NPCs, gRNA 2 increased expression in antibiotic-selected, but not unselected, dCas9^{-VP64} HEK293Ts (Figure S5B). Unexpectedly, *NRXN1* gRNAs 1–6 somewhat increased expression in antibiotic-selected dCas9^{-VP64} HEK293Ts, but not antibiotic-selected

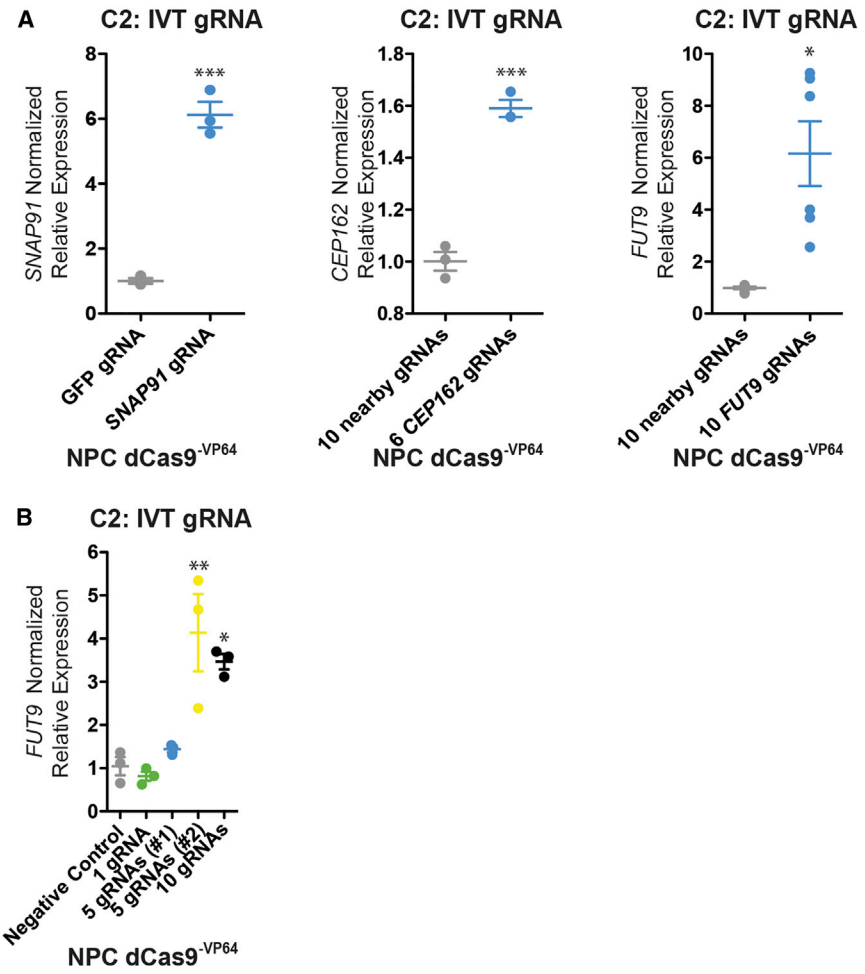

Figure 5. Single and Multiplexed IVT gRNA-Mediated Transcriptional Modulation

(A) Transient expression of IVT gRNAs for transcriptional modulation of *SNAP91* (1 gRNA), *CEP162* (six pooled gRNAs), and *FUT9* (ten pooled gRNAs). Normalized relative mRNA levels (compared with GFP [*SNAP91*] or ten gRNAs targeting a nearby non-promoter non-coding region [*CEP162* and *FUT9*]) following transfection of dCas9^{VP64} NPCs with IVT gRNAs targeted upstream of the TSS for *SNAP91*, *CEP162*, and *FUT9*.

(B) Multiplexed pools of ten, five (two independent pools), and one IVT gRNA(s) for transcriptional modulation of *FUT9*.

Data are presented as means ± SEM (bar graph) from at least three independent biological replicates. Each biological replicate is depicted by a circle. *$p < 0.05$, **$p < 0.01$, ***$p < 0.001$.

dCas9^{-VPR} HEK293Ts (Figures S5C and S5D). Even more unexpectedly, while validated *CLCN3* gRNA 2 increased expression in dCas9^{-VP64} HEK293Ts (Figure S5E), validated *SNAP91* gRNA 3 failed to increase expression in dCas9^{-VP64} HEK293Ts under any conditions (Figure S5F).

We recommend validating gRNA efficacy across not just each individual hiPSC line to be evaluated and each dCas9 effector to be employed, but also each cell type to be characterized.

Non-integrative *In-Vitro*-Transcribed gRNAs Can Substitute for Lentiviral Delivery

Although gRNA-expressing lentiviral vectors efficiently modulate transcription, the cloning and the production of lentiviral particles will likely act as a technical bottleneck as this platform is expanded to higher-throughput applications. For one gene, using *SNAP91* gRNA 3, we tested the efficacy of a transiently expressed *in-vitro*-transcribed (IVT) gRNA to modulate transcription in antibiotic-selected dCas9^{-VP64} NPCs. Forty-eight hours after transfection, we observed robust upregulation of *SNAP91* in NPCs (C2, 6.13-fold, $p < 0.001$; $n = 3$ each; antibiotic selection for dCas9^{-VP64}) (Figure 5A). This magnitude of response was comparable with that achieved by stable lentiviral transduction (Figure 2), suggesting that transient IVT gRNAs might represent a more scalable strategy moving forward. Efficacy of IVT gRNA-mediated transcriptional activation was confirmed across two additional neural genes, *CEP162* (six pooled gRNAs) and *FUT9* (ten pooled gRNAs) (Figure 5A). Finally, we compared the efficacy of pools of ten, five (two independent pools), and one IVT gRNA(s) to modulate transcription in antibiotic-selected dCas9^{-VP64} NPCs. Forty-eight hours after transfection, we observed greatest upregulation of *FUT9* through multiplexing (C2, 10 gRNA pool, 3.3-fold, $p < 0.05$; $n = 3$ each; antibiotic selection for dCas9^{-VP64}) (Figure 5B).

DISCUSSION

Dissecting the function of neuropsychiatric disorder-associated genes will greatly enhance our understanding

of how specific variants contribute to disease risk. While dCas9 effectors are a novel platform for manipulating gene expression, we report a number of practical limitations that must be considered when designing hiPSC-based studies using this promising new tool. First, gRNA efficacies can vary between genes, individuals, neural cell types, and dCas9 effectors. Second, even the rational design of up to six different gRNAs does not guarantee that a functional gRNA will be validated. Moreover, gRNA efficacy seemed to be independent of dCas9 expression levels (data not shown) and/or antibiotic selection for dCas9 vectors (Figures S2 and S4), suggesting there may not be a quick fix to facilitate transcriptional modulation of particularly intransient genes. Consequently, for hiPSC-based functional studies of neuropsychiatric disease risk genes, we advise that the extent of gRNA gene modulation be validated across each individual, cell type, and effector.

Given that such extensive validation would likely increase the time and cost involved in functional studies, and potentially preclude high-throughput analyses, a few alternative strategies might be employed. First, multiplexing many gRNAs in a single vector might increase the likelihood, not only that at least one gRNA is functional, but also that all gRNAs are expressed in each cell, thereby achieving more consistent effects than might be obtained using a pool of gRNA vectors. Second, because IVT gRNAs can substitute for lentiviral delivery, this would reduce the time and costs associated with vector design, construction, and viral packaging, while still being compatible with a multiplex strategy whereby many IVT gRNAs targeting the same gene could be transfected simultaneously. Our hope is that a threshold number of gRNAs will be empirically established, such that when they are combined in a multiplex strategy, there is a high degree of confidence that effective transcriptional modulation across all individuals and cell types of interest will be achieved.

Despite advances in gRNA design algorithms (Chari et al., 2015; Doench et al., 2014, 2016; Xu et al., 2015), gRNA efficacy across individuals, cell types, and dCas9 effectors still must be empirically confirmed. We report clear cell line-dependent effects in gRNA efficacy and hypothesize that epigenetic differences drive this variability across our experiments. There is substantial evidence that the epigenetic landscape impacts gRNA efficacies, including chromatin structure (Chari et al., 2015; Knight et al., 2015; Singh et al., 2015; Wu et al., 2014), nucleosome positioning (Horlbeck et al., 2016b), and DNA methylation (Wu et al., 2014). Histone modifications or competitive interactions with transcriptional machinery may also affect target site accessibility, although so far this has not been as well investigated. Overall, it seems that Cas9 activity is greatest at sites of open chromatin; because chromatin remodeling can restore Cas9 access (Horlbeck et al., 2016b), it is possible that chromatin-modifying enzymes may improve efficacy, although the impact of such treatment on disease-modeling experiments is unknown. It is also possible that alternative and/or combinations of dCas9 effectors acting further from the promoter (Hilton et al., 2015) or that directly modify DNA (Liu et al., 2016) or histone (Kearns et al., 2014) methylation may improve gRNA reliability across genes, individuals, and cell types. Finally, although not tested here, given the reported epigenetic differences between hiPSCs generated from the same individual (Lister et al., 2011; Ma et al., 2014; Mekhoubad et al., 2012; Nazor et al., 2012; Ruiz et al., 2012), it will be interesting to test to what extent gRNA efficacies can vary across isogenic NPCs, neurons, or astrocyte populations differentiated from independent hiPSCs from the same individual; of course, sequencing the promoter regions of each individual at each target gene would be necessary to rule out genetic effects.

Several groups have successfully applied the CRISPR-dCas9 system to modulate gene expression levels for large-scale genome-wide screens (Carlson-Stevermer et al., 2016; Gilbert et al., 2014; Horlbeck et al., 2016a; Konermann et al., 2015). Our findings do not suggest that these dCas9 platforms are unsuitable for genome-wide approaches; rather, we only suggest that when focusing on a small number of candidate genes, it is prudent to always empirically establish the magnitude of gene expression modulation achieved. The successes of these CRISPR screens could reflect technical differences between our approaches (such as the levels of dCas9/gRNA expression, timing of dCas9 and/or gRNA selection, or the biology of specific cell lines used). We do not believe that the variability in gRNA efficacy reflects vector integration effects (such as differences in copy number or expression levels of dCas9 and/or gRNAs), as our FACS (Figure S2A) and qPCR (Figures S2B and S2C) data suggest that the difference in dCas9 expression across individuals is small, an observation that is consistent with findings that dCas9^{-KRAB} expression does not correlate to the level of changes gene expression achieved (Dixit et al., 2016). The generation of antibiotic selection of stable lines expressing dCas9^{-VPR}, dCas9^{-KRAB}, and dCas9-VP64 sometimes, but not always, improved gRNA efficacy in our hands. Owing to high transduction efficiencies observed with our (small) gRNA expression vectors, we did not test the impact of gRNA selection; nonetheless, it is possible that gRNA selection is a critical variable and/or that the timing of selection is important such that dCas9-effector and gRNA selection is more appropriately conducted concurrently instead of sequentially. More likely, the solution may simply entail multiplexing a variety of gRNAs simultaneously (Figures 4E and 5B).

We were particularly interested in the synthetic activation of gene expression from the *NRNX1* locus, given the

size and diverse alternative splice repertoire of its gene products; we were surprised at our inability to increase expression. We can only speculate that known (Runkel et al., 2013) or unknown epigenetic effects near the *NRXN1* promoter prevented us from increasing expression of this key neural gene in NPCs. Numerous factors have been hypothesized to affect gRNA efficacy for genome-editing purposes, including nucleosome positioning and 3D genome architecture of different cell types (Smith et al., 2016), which can limit access of the gRNA to the target site. As our understanding of the epigenome grows, and with it our ability to better predict gRNA targets, we hope that dCas9-mediated transcriptional modulation will become a more robust and scalable technology.

EXPERIMENTAL PROCEDURES

gRNA Design and Cloning

gRNAs were designed using either the optimized CRISPR (http://crispr.mit.edu/) or the CRISPR-ERA (http://crispr-era.stanford.edu) web tools. gRNAs were selected based on their specific locations at decreasing distances from the TSS as well as their lack of predicted off targets and E scores (http://crispr-era.stanford.edu). For lentiviral cloning: synthesized oligonucleotides (Thermo Fisher Scientific; Table S2) were annealed (37°C for 30 min, 95°C for 5 min, ramp-down to 25°C at 5°C per min), diluted 1:100 and then ligated into BsmB1-digested lentiGuide-dTomato or lentiGuide-mTagBFP2-Puro (described below). For IVT production: PCR assembly of gRNA DNA template using synthetic forward and reverse oligonucleotides for SNAP91 (Table S2) with the Tracr Fragment + T7 Primer Mix was performed as per GeneArt Precision gRNA Synthesis Kit (Thermo Fisher Scientific, A29377) instructions. The *SNAP91* gRNA was generated by *in vitro* transcription and purified as per the GeneArt Precision gRNA Synthesis Kit instructions.

Gibson Assembly of Vectors

Unless specified, all cloning reagents were from NEB and plasmid backbones were from Addgene (https://www.addgene.org/). Primers were synthesized by Thermo Fisher Scientific. All fragments were assembled using NEBuilder HiFi DNA Assembly Master Mix (NEB, no. E2621X). All assemblies were transformed into either DH5α Extreme Efficiency Competent Cells (Allele Biotechnology, no. ABP-CE-CC02050) or Stbl3 Chemically Competent *E. coli* (Thermo Fisher Scientific, no. C737303). Positive clones were confirmed by restriction digest and Sanger sequencing (GENEWIZ).

The following vectors have been deposited at Addgene: lenti-EF1a-dCas9^{-VP64}-Puro, lenti-EF1a-dCas9^{-VPR}-Puro, lenti-EF1a-dCas9^{-KRAB}-Puro, lentiGuide-Hygro-mTagBFP2, lentiGuide-Hygro-eGFP, lentiGuide-Hygro-dTomato, lentiGuide-Hygro-iRFP670, and pLV-TetO-h*NGN2*-Neo.

lentiGuide-dTomato and lentiGuide-mTagBFP2-Hygro

lentiGuide-Puro (Addgene, no. 52963) was digested with Mlu1 and BsiWI. dTomato was amplified from AAV-hSyn1-GCaMP6f-P2A-NLS-dTomato (Addgene, no.51085). HygroR sequence was amplified from lenti MS2-P65-HSF1_Hygro (Addgene, no. 61426). mTagBFP2 was amplified form pBAD-mTagBFP2 (Addgene, no. 3463). The P2A self-cleaving peptide sequence was amplified using a reverse primer of HygroR and forward primer of mTagBFP2. All gRNA sequences are provided in Table S2.

Lentiviral dCas9 Effectors

To engineer a lentiviral transfer vector that expresses dCas9:VP64-T2A-Puro (EF1a-NLS-dCas9(N863)-VP64-T2A-Puro-WPRE), dCas9:VP64-T2A-Blast (EF1a-NLS-dCas9(N863)-VP64-T2A-Blast-WPRE) (Addgene, no. 61,425) was digested with BsrGI and EcoRI. T2A-PuroR was amplified from pLV-TetO-hNGN2-P2A-eGFP-T2A-Puro (Addgene, no. 79823). Fragments were then assembled using NEBuilder HiFi DNA Assembly Master Mix (NEB, no. E2621). To engineer a lentiviral transfer vector that expresses dCas9:KRAB-Puro (EF1a-NLS-dCas9(N863)-KRAB-T2A-Puro-WPRE), dCas9:VP64-T2A-Blast (EF1a-NLS-dCas9(N863)-VP64-T2A-Blast-WPRE) (Addgene, no.61425) was first digested with BamHI and BsrGI. KRAB was then amplified from pHAGE-TRE-dCas9:KRAB (Addgene, no. 50917). Fragments were then assembled using NEBuilder HiFi DNA Assembly Master Mix. dCas9:KRAB-Blast was digested with BsrGI and EcoRI, and T2A-PuroR was amplified from pLV-TetO-hNGN2-P2A-eGFP-T2A-Puro (Addgene, no. 79823). Fragments were then assembled using NEBuilder HiFi DNA Assembly Master Mix. To engineer a lentiviral transfer vector that expresses dCas9:VPR-Puro (EF1a-NLS-dCas9(D10A, D839A, H840A, and N863A)-VPR-T2A-Puro-WPRE), dCas9:VPR was first amplified from SP-dCas9-VPR (Addgene, no. 63798), and T2A-PuroR was amplified from pLV-TetO-hNGN2-P2A-eGFP-T2A-Puro (Addgene, no. 79823). dCas9:KRAB-T2A-Puro was digested with BsiWI and EcoRI. Fragments were then assembled using NEBuilder HiFi DNA Assembly Master Mix.

Lentivirus Generation

Lentiviruses were produced as described previously (Brennand et al., 2011; Ho et al., 2016). The lentiviral constructs expressing dCas9:VP64-T2A-Puro or dCas9:VPR-T2A-Puro or dCas9:KRAB-T2A-Puro (EF1α-dCas9:VP64-T2A-Puro or EF1α-dCas9:VPR-T2A-Puro or EF1α-dCas9:KRAB-T2A-Puro, respectively) are described above. Physical titration of lentivirus was performed by qPCR (qPCR Lentivirus Titration [Titer] Kit, ABMgood, no. LV900).

Generation of Antibiotic-Selected dCas9-VP64, dCas9-VPR, and dCas9-KRAB NPCs

NPCs per well (3.0×10^6) were seeded onto growth factor-reduced Matrigel-coated six-well plates in NPC medium. The following day, lentiviruses generated as above using either the lentiviral vectors dCas9:VP64-T2A-Puro, dCas9:VPR-T2A-Puro, and dCas9:KRAB-T2A-Puro were added, and cultures were spinfected (1 hr, 1,000 × *g*, 25°C). Following spinfection, plates were transferred to a cell culture incubator for 3 hr. Medium was then removed and replaced with fresh NPC medium. Two days later, fresh NPC medium containing 1 μg/mL puromycin (Sigma, no. P7255) was added and cells were expanded in NPC medium containing 1 μg/mL puromycin followed by banking in liquid nitrogen. Once thawed, NPCs were grown in NPC medium containing 1 μg/mL puromycin for the remainder of the experiment. Antibiotic-selected NPC lines were validated via FACS using an antibody for Cas9. Vendors, catalog numbers, and dilutions of all antibodies used are listed in Table S4.

Transduction of dCas9-Effector NPCs with gRNA Lentivirus

dCas9-effector NPCs per well (3.5×10^5) were seeded onto growth factor-reduced Matrigel-coated 24-well plates in NPC medium containing 1 μg/mL puromycin. The next day, lentiviruses generated as above were added and cultures were spinfected (1 hr, 1,000 × *g*, 25°C). Following spinfection, plates were transferred to a cell culture incubator for 3 hr. The medium was then removed and replaced with fresh NPC medium containing 1 μg/mL puromycin. Cells were harvested 48 hr later.

Transduction of Antibiotic-Selected dCas9-VP64 NPC-Astrocytes with gRNA Lentivirus

Antibiotic-selected dCas9-VP64 NPC-astrocytes per well (1×10^5) were seeded onto growth factor-reduced Matrigel-coated 24-well plates in Astrocyte medium containing 1 μg/mL puromycin. The next day, lentiviruses generated as above were added and cultures were spinfected (1 hr, 1,000 × *g*, 25°C). Following spinfection, plates were transferred to a cell culture incubator for 3 hr. Medium was then removed and replaced with fresh Astrocyte medium containing 1 μg/mL puromycin. Cells were harvested 48 hr later.

Transfection of Antibiotic-Selected dCas9-Effector NPCs with IVT gRNA

Antibiotic-selected dCas9-effector NPCs per well (4.0×10^5) were added to growth factor-reduced Matrigel-coated 24-well plates in NPC medium containing 1 μg/mL puromycin. *SNAP91* gRNA#2 IVT product (600 ng) and 2 μL of EditPro Stem Transfection Reagent (MTI-GlobalStem, no. GST-2174), diluted in 50 μL of Opti-MEM (Thermo Fisher Scientific, no. 31985062) was added drop wise directly after. Cells were harvested 48 hr later.

Real-Time qPCR

Total RNA was extracted using TRIzol following the manufactures instructions. Transcript analysis was carried out using a QuantStudio 7 Flex Real-Time PCR System using the Power SYBR Green RNA-to-Ct Real-Time qPCR Kit for primers (all Thermo Fisher Scientific). RNA template (50 ng) was added to the PCR mix, containing primers detailed in Table S3 (Thermo Fisher Scientific). qPCR conditions were as follows, 48°C for 15 min, 95°C for 10 min followed by 40 cycles (95°C for 15 s, 60°C for 60 s).

Live-Cell Fluorescent Protein Detection

Cells were dissociated using Accutase, washed with DMEM, and resuspended in FACS buffer (1× PBS [without Mg^{2+}/Ca^{2}] containing 1%, v/v, BSA and TO-PRO3 [1 μM, Thermo Fisher Scientific] and filtered using a 40-μm filter [BD Biosciences]). Cytometry was performed using an LSR II or FACS Canto (BD Biosciences) and analysis was performed using FlowJo (v.8.7.3, Tree Star).

Data Analysis

All qPCR data represent at least three independent biological experiments. Data were analyzed using GraphPad Prism 6 software. Values are expressed as means ± SEM. Statistical significance was tested using one-way ANOVA with Tukey's *post hoc* test for comparison of all sample means. *$p < 0.05$, **$p < 0.01$, ***$p < 0.001$, ****$p < 0.0001$.

Human subjects work on these de-identified control hiPSCs was approved by the Institutional Review Board at Icahn School of Medicine.

SUPPLEMENTAL INFORMATION

Supplemental Information includes Supplemental Experimental Procedures, five figures, and four tables and can be found with this article online at http://dx.doi.org/10.1016/j.stemcr.2017.06.012.

AUTHOR CONTRIBUTIONS

S.M.H., B.J.H., E.F., P.R., and K.J.B. contributed to the experimental design. S.M.H., B.J.H., E.F., and P.R. completed all cell culture experiments. E.F. cloned gRNAs. S.M.H., B.J.H., E.F., P.R., R.A., N.B., and H.M. performed qPCR and data analysis. I.O. completed western blot analysis. H.P. and S.A. provided critical assistance. S.M.H., B.J.H., and K.J.B. wrote the manuscript.

ACKNOWLEDGMENTS

Kristen J. Brennand is a New York Stem Cell Foundation—Robertson Investigator. The Brennand Laboratory is supported by a Brain and Behavior Young Investigator Grant, NIH grants R01 MH101454 and R01 MH106056, and the New York Stem Cell Foundation. We thank the FACS core at Icahn School of Medicine at Mount Sinai.

All vectors generated for this manuscript have been deposited with Addgene.

Received: March 23, 2017
Revised: June 23, 2017
Accepted: June 24, 2017
Published: July 27, 2017

REFERENCES

Brennand, K.J., Simone, A., Jou, J., Gelboin-Burkhart, C., Tran, N., Sangar, S., Li, Y., Mu, Y., Chen, G., Yu, D., et al. (2011). Modelling schizophrenia using human induced pluripotent stem cells. Nature *473*, 221–225.

Brennand, K., Savas, J.N., Kim, Y., Tran, N., Simone, A., Hashimoto-Torii, K., Beaumont, K.G., Kim, H.J., Topol, A., Ladran, I., et al. (2015). Phenotypic differences in hiPSC NPCs derived from patients with schizophrenia. Mol. Psychiatry *20*, 361–368.

Carcamo-Orive, I., Hoffman, G.E., Cundiff, P., Beckmann, N.D., D'Souza, S.L., Knowles, J.W., Patel, A., Papatsenko, D., Abbasi, F., Reaven, G.M., et al. (2017). Analysis of transcriptional variability in a large human iPSC library reveals genetic and non-genetic determinants of heterogeneity. Cell Stem Cell *20*, 518–532.e9.

Carlson-Stevermer, J., Goedland, M., Steyer, B., Movaghar, A., Lou, M., Kohlenberg, L., Prestil, R., and Saha, K. (2016). High-content analysis of CRISPR-Cas9 gene-edited human embryonic stem cells. Stem Cell Reports *6*, 109–120.

Chari, R., Mali, P., Moosburner, M., and Church, G.M. (2015). Unraveling CRISPR-Cas9 genome engineering parameters via a library-on-library approach. Nat. Methods *12*, 823–826.

Chavez, A., Scheiman, J., Vora, S., Pruitt, B.W., Tuttle, M., P R Iyer, E., Lin, S., Kiani, S., Guzman, C.D., et al. (2015). Highly efficient Cas9-mediated transcriptional programming. Nat. Methods *12*, 326–328.

Chavez, A., Tuttle, M., Pruitt, B.W., Ewen-Campen, B., Chari, R., Ter-Ovanesyan, D., Haque, S.J., Cecchi, R.J., Kowal, E.J., Buchthal, J., et al. (2016). Comparison of Cas9 activators in multiple species. Nat. Methods *13*, 563–567.

Cong, L., Ran, F.A., Cox, D., Lin, S., Barretto, R., Habib, N., Hsu, P.D., Wu, X., Jiang, W., Marraffini, L.A., et al. (2013). Multiplex genome engineering using CRISPR/Cas systems. Science *339*, 819–823.

CNV and Schizophrenia Working Groups of the Psychiatric Genomics Consortium; Psychosis Endophenotypes International Consortium (2017). Contribution of copy number variants to schizophrenia from a genome-wide study of 41,321 subjects. Nat. Genet. *49*, 27–35.

Dixit, A., Parnas, O., Li, B., Chen, J., Fulco, C.P., Jerby-Arnon, L., Marjanovic, N.D., Dionne, D., Burks, T., Raychowdhury, R., et al. (2016). Perturb-seq: dissecting molecular circuits with scalable single-cell RNA profiling of pooled genetic screens. Cell *167*, 1853–1866.e17.

Doench, J.G., Hartenian, E., Graham, D.B., Tothova, Z., Hegde, M., Smith, I., Sullender, M., Ebert, B.L., Xavier, R.J., and Root, D.E. (2014). Rational design of highly active sgRNAs for CRISPR-Cas9-mediated gene inactivation. Nat. Biotechnol. *32*, 1262–1267.

Doench, J.G., Fusi, N., Sullender, M., Hegde, M., Vaimberg, E.W., Donovan, K.F., Smith, I., Tothova, Z., Wilen, C., Orchard, R., et al. (2016). Optimized sgRNA design to maximize activity and minimize off-target effects of CRISPR-Cas9. Nat. Biotechnol. *34*, 184–191.

Fromer, M., Roussos, P., Sieberts, S.K., Johnson, J.S., Kavanagh, D.H., Perumal, T.M., Ruderfer, D.M., Oh, E.C., Topol, A., Shah, H.R., et al. (2016). Gene expression elucidates functional impact of polygenic risk for schizophrenia. Nat. Neurosci. *19*, 1442–1453.

Gilbert, L.A., Larson, M.H., Morsut, L., Liu, Z., Brar, G.A., Torres, S.E., Stern-Ginossar, N., Brandman, O., Whitehead, E.H., Doudna, J.A., et al. (2013). CRISPR-mediated modular RNA-guided regulation of transcription in eukaryotes. Cell *154*, 442–451.

Gilbert, L.A., Horlbeck, M.A., Adamson, B., Villalta, J.E., Chen, Y., Whitehead, E.H., Guimaraes, C., Panning, B., Ploegh, H.L., Bassik, M.C., et al. (2014). Genome-scale CRISPR-mediated control of gene repression and activation. Cell *159*, 647–661.

Hilton, I.B., D'Ippolito, A.M., Vockley, C.M., Thakore, P.I., Crawford, G.E., Reddy, T.E., and Gersbach, C.A. (2015). Epigenome editing by a CRISPR-Cas9-based acetyltransferase activates genes from promoters and enhancers. Nat. Biotechnol. *33*, 510–517.

Ho, S.M., Hartley, B.J., TCW, J., Beaumont, M., Stafford, K., Slesinger, P.A., and Brennand, K.J. (2016). Rapid Ngn2-induction of excitatory neurons from hiPSC-derived neural progenitor cells. Methods *101*, 113–124.

Horlbeck, M.A., Gilbert, L.A., Villalta, J.E., Adamson, B., Pak, R.A., Chen, Y., Fields, A.P., Park, C.Y., Corn, J.E., Kampmann, M., et al. (2016a). Compact and highly active next-generation libraries for CRISPR-mediated gene repression and activation. Elife *5*. http://dx.doi.org/10.7554/eLife.19760.

Horlbeck, M.A., Witkowsky, L.B., Guglielmi, B., Replogle, J.M., Gilbert, L.A., Villalta, J.E., Torigoe, S.E., Tjian, R., and Weissman, J.S. (2016b). Nucleosomes impede Cas9 access to DNA *in vivo* and *in vitro*. Elife *5*. http://dx.doi.org/10.7554/eLife.12677.

Isaac, R.S., Jiang, F., Doudna, J.A., Lim, W.A., Narlikar, G.J., and Almeida, R. (2016). Nucleosome breathing and remodeling constrain CRISPR-Cas9 function. Elife *5*. http://dx.doi.org/10.7554/eLife.13450.

Jaaro-Peled, H., Ayhan, Y., Pletnikov, M.V., and Sawa, A. (2010). Review of pathological hallmarks of schizophrenia: comparison of genetic models with patients and nongenetic models. Schizophr. Bull. *36*, 301–313.

Jiang, C., and Pugh, B.F. (2009). Nucleosome positioning and gene regulation: advances through genomics. Nat. Rev. Genet. *10*, 161–172.

Jinek, M., Chylinski, K., Fonfara, I., Hauer, M., Doudna, J.A., and Charpentier, E. (2012). A programmable dual-RNA-guided DNA endonuclease in adaptive bacterial immunity. Science *337*, 816–821.

Kearns, N.A., Genga, R.M., Enuameh, M.S., Garber, M., Wolfe, S.A., and Maehr, R. (2014). Cas9 effector-mediated regulation of transcription and differentiation in human pluripotent stem cells. Development *141*, 219–223.

Knight, S.C., Xie, L., Deng, W., Guglielmi, B., Witkowsky, L.B., Bosanac, L., Zhang, E.T., El Beheiry, M., Masson, J.B., Dahan, M., et al. (2015). Dynamics of CRISPR-Cas9 genome interrogation in living cells. Science *350*, 823–826.

Konermann, S., Brigham, M.D., Trevino, A.E., Joung, J., Abudayyeh, O.O., Barcena, C., Hsu, P.D., Habib, N., Gootenberg, J.S., Nishimasu, H., et al. (2015). Genome-scale transcriptional activation by an engineered CRISPR-Cas9 complex. Nature *517*, 583–588.

Lin, M., Pedrosa, E., Hrabovsky, A., Chen, J., Puliafito, B.R., Gilbert, S.R., Zheng, D., and Lachman, H.M. (2016). Integrative transcriptome network analysis of iPSC-derived neurons from schizophrenia and schizoaffective disorder patients with 22q11.2 deletion. BMC Syst. Biol. *10*, 105.

Lister, R., Pelizzola, M., Kida, Y.S., Hawkins, R.D., Nery, J.R., Hon, G., Antosiewicz-Bourget, J., O'Malley, R., Castanon, R., Klugman, S., et al. (2011). Hotspots of aberrant epigenomic reprogramming in human induced pluripotent stem cells. Nature *471*, 68–73.

Liu, X.S., Wu, H., Ji, X., Stelzer, Y., Wu, X., Czauderna, S., Shu, J., Dadon, D., Young, R.A., and Jaenisch, R. (2016). Editing DNA methylation in the mammalian genome. Cell *167*, 233–247.e217.

Ma, H., Morey, R., O'Neil, R.C., He, Y., Daughtry, B., Schultz, M.D., Hariharan, M., Nery, J.R., Castanon, R., Sabatini, K., et al. (2014). Abnormalities in human pluripotent cells due to reprogramming mechanisms. Nature *511*, 177–183.

Maeder, M.L., Linder, S.J., Cascio, V.M., Fu, Y., Ho, Q.H., and Joung, J.K. (2013). CRISPR RNA-guided activation of endogenous human genes. Nat. Methods *10*, 977–979.

Maillard, A.M., Ruef, A., Pizzagalli, F., Migliavacca, E., Hippolyte, L., Adaszewski, S., Dukart, J., Ferrari, C., Conus, P., Mannik, K., et al. (2015). The 16p11.2 locus modulates brain structures common to autism, schizophrenia and obesity. Mol. Psychiatry *20*, 140–147.

McDonald, J.I., Celik, H., Rois, L.E., Fishberger, G., Fowler, T., Rees, R., Kramer, A., Martens, A., Edwards, J.R., and Challen, G.A. (2016). Reprogrammable CRISPR/Cas9-based system for inducing site-specific DNA methylation. Biol. Open *5*, 866–874.

Mekhoubad, S., Bock, C., de Boer, A.S., Kiskinis, E., Meissner, A., and Eggan, K. (2012). Erosion of dosage compensation impacts human iPSC disease modeling. Cell Stem Cell *10*, 595–609.

Nazor, K.L., Altun, G., Lynch, C., Tran, H., Harness, J.V., Slavin, I., Garitaonandia, I., Muller, F.J., Wang, Y.C., Boscolo, F.S., et al. (2012). Recurrent variations in DNA methylation in human pluripotent stem cells and their differentiated derivatives. Cell Stem Cell *10*, 620–634.

Nishizawa, M., Chonabayashi, K., Nomura, M., Tanaka, A., Nakamura, M., Inagaki, A., Nishikawa, M., Takei, I., Oishi, A., Tanabe, K., et al. (2016). Epigenetic variation between human induced pluripotent stem cell lines is an indicator of differentiation capacity. Cell Stem Cell *19*, 341–354.

Qi, L.S., Larson, M.H., Gilbert, L.A., Doudna, J.A., Weissman, J.S., Arkin, A.P., and Lim, W.A. (2013). Repurposing CRISPR as an RNA-guided platform for sequence-specific control of gene expression. Cell *152*, 1173–1183.

Rouhani, F., Kumasaka, N., de Brito, M.C., Bradley, A., Vallier, L., and Gaffney, D. (2014). Genetic background drives transcriptional variation in human induced pluripotent stem cells. PLoS Genet. *10*, e1004432.

Ruiz, S., Diep, D., Gore, A., Panopoulos, A.D., Montserrat, N., Plongthongkum, N., Kumar, S., Fung, H.L., Giorgetti, A., Bilic, J., et al. (2012). Identification of a specific reprogramming-associated epigenetic signature in human induced pluripotent stem cells. Proc. Natl. Acad. Sci. USA *109*, 16196–16201.

Runkel, F., Rohlmann, A., Reissner, C., Brand, S.M., and Missler, M. (2013). Promoter-like sequences regulating transcriptional activity in neurexin and neuroligin genes. J. Neurochem. *127*, 36–47.

Schizophrenia Working Group of the Psychiatric Genomics Consortium (2014). Biological insights from 108 schizophrenia-associated genetic loci. Nature *511*, 421–427.

Singh, R., Kuscu, C., Quinlan, A., Qi, Y., and Adli, M. (2015). Cas9-chromatin binding information enables more accurate CRISPR off-target prediction. Nucleic Acids Res. *43*, e118.

Smith, J.D., Suresh, S., Schlecht, U., Wu, M., Wagih, O., Peltz, G., Davis, R.W., Steinmetz, L.M., Parts, L., and St Onge, R.P. (2016). Quantitative CRISPR interference screens in yeast identify chemical-genetic interactions and new rules for guide RNA design. Genome Biol. *17*, 45.

Srikanth, P., Han, K., Callahan, D.G., Makovkina, E., Muratore, C.R., Lalli, M.A., Zhou, H., Boyd, J.D., Kosik, K.S., Selkoe, D.J., et al. (2015). Genomic DISC1 disruption in hiPSCs alters Wnt signaling and neural cell fate. Cell Rep. *12*, 1414–1429.

TCW, J., Wang, M., Pimenova, A.A., Bowles, K.R., Hartley, B.J., Lacin, E., Machlovi, S., Abdelaal, R., Karch, C.M., et al. (2017). An efficient platform for astrocyte differentiation from human induced pluripotent stem cells. bioRxiv http://dx.doi.org/10.1101/133496.

Thakore, P.I., D'Ippolito, A.M., Song, L., Safi, A., Shivakumar, N.K., Kabadi, A.M., Reddy, T.E., Crawford, G.E., and Gersbach, C.A. (2015). Highly specific epigenome editing by CRISPR-Cas9 repressors for silencing of distal regulatory elements. Nat. Methods *12*, 1143–1149.

Topol, A., English, J.A., Flaherty, E., Rajarajan, P., Hartley, B.J., Gupta, S., Desland, F., Zhu, S., Goff, T., Friedman, L., et al. (2015). Increased abundance of translation machinery in stem cell-derived neural progenitor cells from four schizophrenia patients. Transl. Psychiatry *5*, e662.

Topol, A., Zhu, S., Hartley, B.J., English, J., Hauberg, M.E., Tran, N., Rittenhouse, C.A., Simone, A., Ruderfer, D.M., Johnson, J., et al. (2016). Dysregulation of miRNA-9 in a subset of schizophrenia patient-derived neural progenitor cells. Cell Rep. *15*, 1024–1036.

Vojta, A., Dobrinic, P., Tadic, V., Bockor, L., Korac, P., Julg, B., Klasic, M., and Zoldos, V. (2016). Repurposing the CRISPR-Cas9 system for targeted DNA methylation. Nucleic Acids Res. *44*, 5615–5628.

Wen, Z., Nguyen, H.N., Guo, Z., Lalli, M.A., Wang, X., Su, Y., Kim, N.S., Yoon, K.J., Shin, J., Zhang, C., et al. (2014). Synaptic dysregulation in a human iPS cell model of mental disorders. Nature *515*, 414–418.

Wong, A.H.C., and Van Tol, H.H.M. (2003). Schizophrenia: from phenomenology to neurobiology. Neurosci. Biobehav. Rev. *27*, 269–306.

Wu, X., Scott, D.A., Kriz, A.J., Chiu, A.C., Hsu, P.D., Dadon, D.B., Cheng, A.W., Trevino, A.E., Konermann, S., Chen, S., et al. (2014). Genome-wide binding of the CRISPR endonuclease Cas9 in mammalian cells. Nat. Biotechnol. *32*, 670–676.

Xu, H., Xiao, T., Chen, C.H., Li, W., Meyer, C.A., Wu, Q., Wu, D., Cong, L., Zhang, F., Liu, J.S., et al. (2015). Sequence determinants of improved CRISPR sgRNA design. Genome Res. *25*, 1147–1157.

Xu, M., Lee, E.M., Wen, Z., Cheng, Y., Huang, W.K., Qian, X., Tcw, J., Kouznetsova, J., Ogden, S.C., Hammack, C., et al. (2016). Identification of small-molecule inhibitors of Zika virus infection and induced neural cell death via a drug repurposing screen. Nat. Med. *22*, 1101–1107.

Yoon, K.J., Nguyen, H.N., Ursini, G., Zhang, F., Kim, N.S., Wen, Z., Makri, G., Nauen, D., Shin, J.H., Park, Y., et al. (2014). Modeling a genetic risk for schizophrenia in iPSCs and mice reveals neural stem cell deficits associated with adherens junctions and polarity. Cell Stem Cell *15*, 79–91.

Yu, D.X., Di Giorgio, F.P., Yao, J., Marchetto, M.C., Brennand, K., Wright, R., Mei, A., McHenry, L., Lisuk, D., Grasmick, J.M., et al. (2014). Modeling hippocampal neurogenesis using human pluripotent stem cells. Stem Cell Reports *2*, 295–310.

Zhang, Y., Pak, C., Han, Y., Ahlenius, H., Zhang, Z., Chanda, S., Marro, S., Patzke, C., Acuna, C., Covy, J., et al. (2013). Rapid single-step induction of functional neurons from human pluripotent stem cells. Neuron *78*, 785–798.

Zhang, Y., Sloan, S.A., Clarke, L.E., Caneda, C., Plaza, C.A., Blumenthal, P.D., Vogel, H., Steinberg, G.K., Edwards, M.S., Li, G., et al. (2016). Purification and characterization of progenitor and mature human astrocytes reveals transcriptional and functional differences with mouse. Neuron *89*, 37–53.

Zhao, D., Lin, M., Chen, J., Pedrosa, E., Hrabovsky, A., Fourcade, H.M., Zheng, D., and Lachman, H.M. (2015). MicroRNA profiling of neurons generated using induced pluripotent stem cells derived from patients with schizophrenia and schizoaffective disorder, and 22q11.2 Del. PLoS One *10*, e0132387.

Stem Cell Reports, Volume *9*

Supplemental Information

Evaluating Synthetic Activation and Repression of Neuropsychiatric-Related Genes in hiPSC-Derived NPCs, Neurons, and Astrocytes

Seok-Man Ho, Brigham J. Hartley, Erin Flaherty, Prashanth Rajarajan, Rawan Abdelaal, Ifeanyi Obiorah, Natalie Barretto, Hamza Muhammad, Hemali P. Phatnani, Schahram Akbarian, and Kristen J. Brennand

SUPPLEMENTAL INFORMATION

SUPPLEMENTAL FIGURES

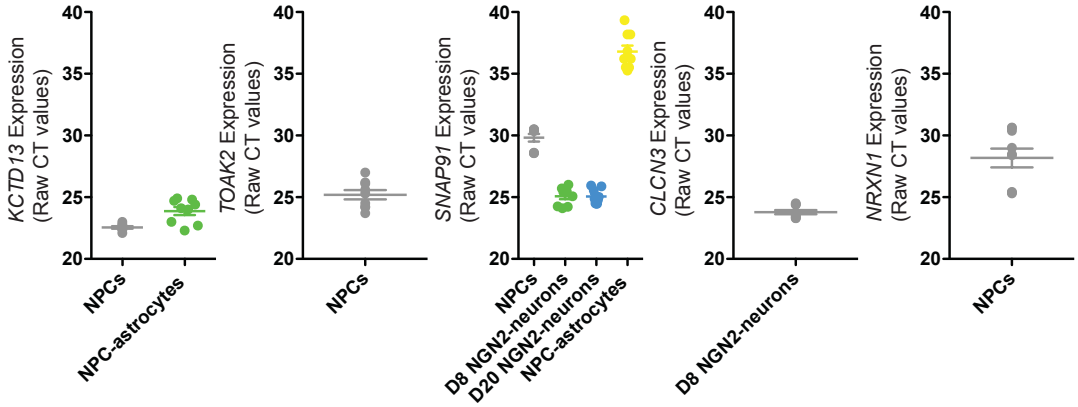

SI Figure 1. Baseline cell-type specific expression of SZ genes. Raw CT scores indicating baseline *KCTD13, TOAK2, NRXN1, SNAP91* and *CLCN3* mRNA levels in NPCs (grey), 8-day *NGN2*-neurons (green), 20-day *NGN2*-neurons (blue) and NPC-astrocytes (yellow), as appropriate for the cell types evaluated for each gene. Data are presented as mean ± s.e.m (bar graph) from at least 3 independent biological replicates. Each biological replicate is depicted by a circle.

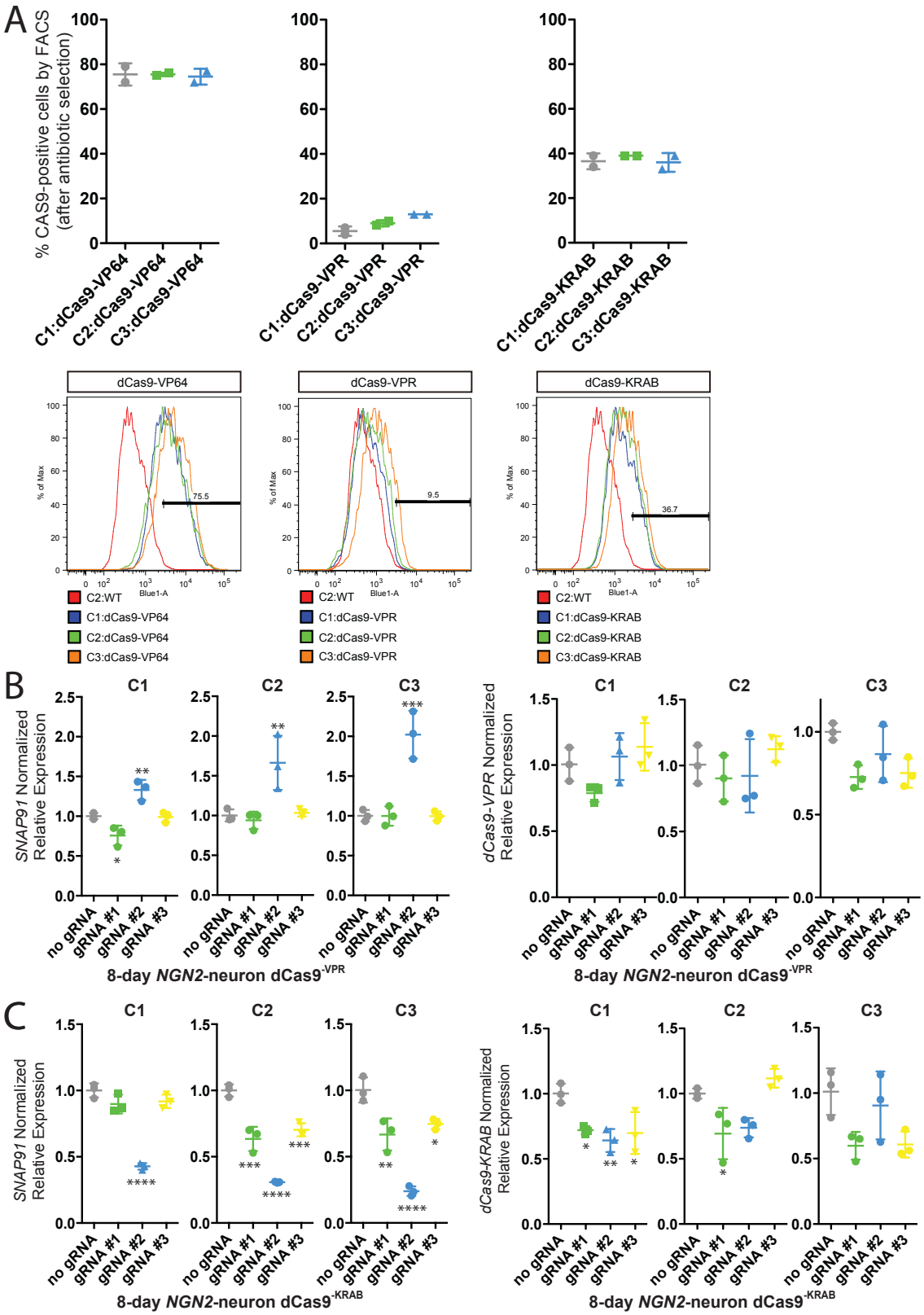

SI Figure 2. Evaluation of dCas9 expression and protein levels. **A.** FACS analysis of

Cas9 protein in antibiotic selected dCas9$^{-VP16,}$ dCas9$^{-VPR\ and}$ dCas9^{-KRAB} NPC lines, shown as graphs (top) and histogram plots (bottom). **B-C.** Normalized relative *SNAP91*:*dCas9* mRNA levels (compared to scrambled gRNA control (grey)) following transduction of dCas9^{VPR} (**B**) and dCas9^{KRAB} (**C**) 8-day NGN2-neurons with lentivirus expressing gRNAs targeted to three different locations (green, blue, yellow) upstream of the TSS for *SNAP91*. Data are presented as mean ± s.e.m (bar graph) from at least 3 independent biological replicates. Each biological replicate is depicted by a circle. *=$p < 0.05$, **=$p < 0.01$, ***=$p < 0.001$, ****=$p < 0.0001$.

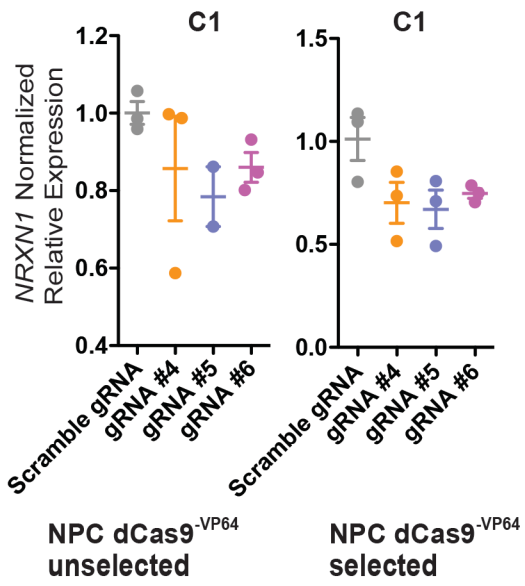

SI Figure 3. Evaluation of impact of antibiotic selection for dCas9-VP64 on gRNA efficacy. Normalized relative mRNA levels (compared to scrambled gRNA control (grey)) following transduction of dCas9^{VP64} NPCs with lentivirus expressing gRNAs targeted to three different locations (green, blue, yellow) upstream of the TSS for *NRXN1*. Data are presented as mean ± s.e.m (bar graph) from at least 3 independent biological replicates. Each biological replicate is depicted by a circle.

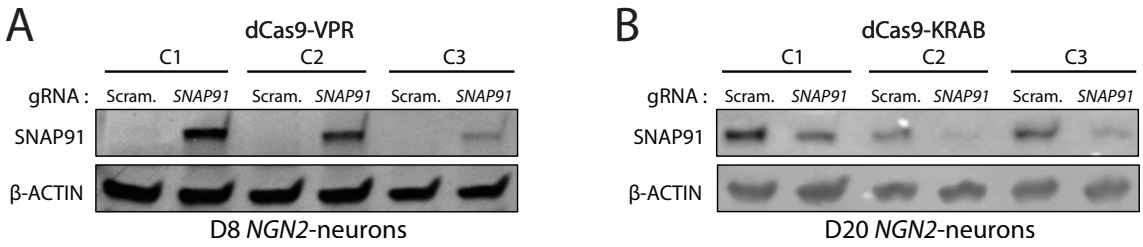

SI Figure 4. Evaluation of changes in SNAP91 protein levels by dCas9^{VP64} in NPCs. A. Representative western blots following transduction of dCas9^{VPR} NPCs with lentivirus expressing *SNAP91* gRNA#2, day 8 *NGN2*-neurons. **B.** Representative western blots following transduction of dCas9^{KRAB} NPCs with lentivirus expressing *SNAP91* gRNA#2, day 21 *NGN2*-neurons.

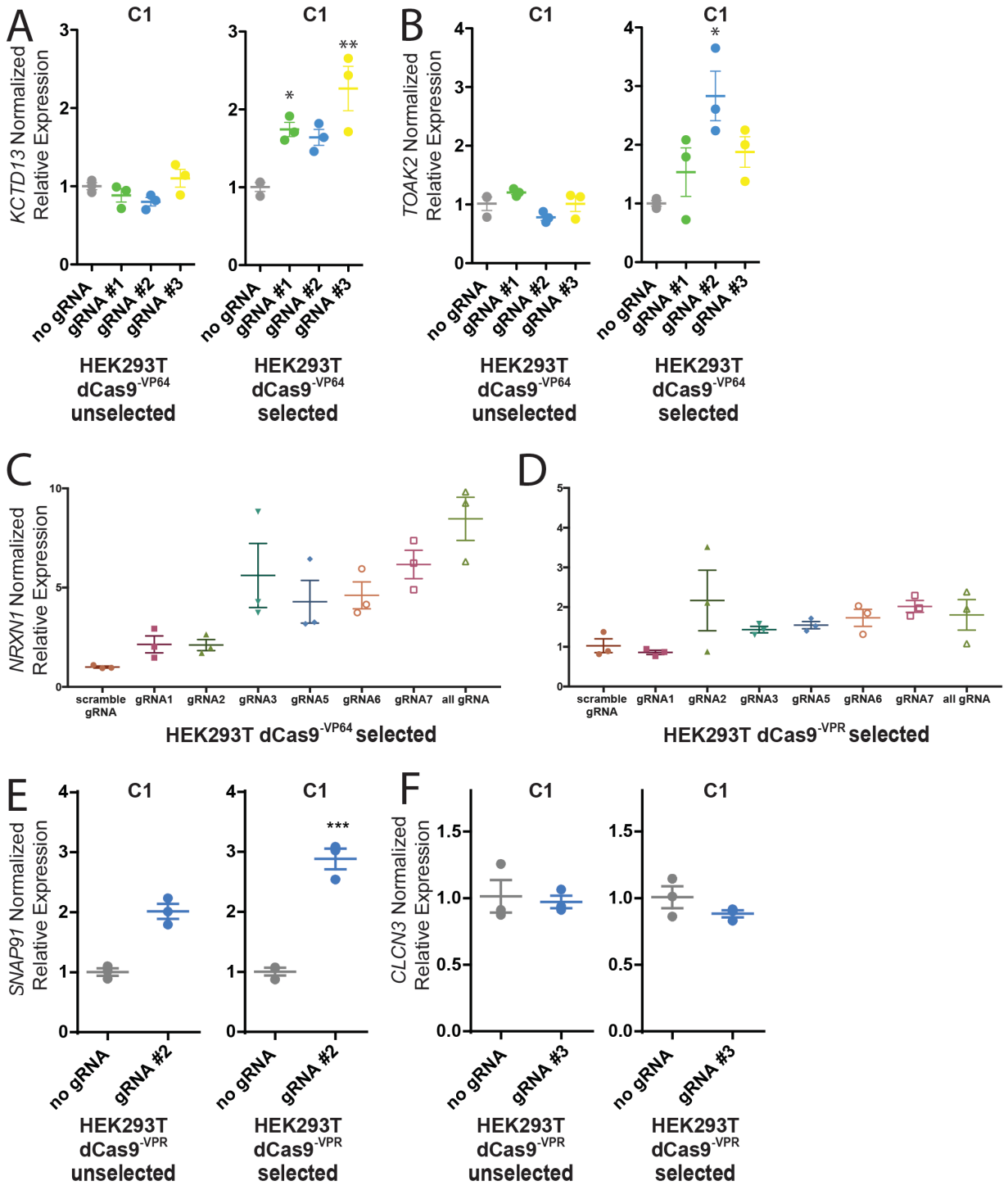

SI Figure 5. Evaluation of impact of gRNA efficacy in HEK293Ts. A-D. Normalized relative mRNA levels (compared to scrambled gRNA control (grey)) following transduction of antibiotic-selected and/or non-selected dCas9^{VP64} (**A-C**) and dCas9^{VPR} (**D-F**) HEK293Ts with lentivirus expressing gRNAs targeted to three to six different locations (green, blue, yellow, orange, purple and pink) upstream of the TSS for *KCTD13* (**A**), *TOAK2* (**B**), *NRXN1*

(**C-D**), *SNAP91* (**E**) and *CLCN3* (**F**). Data are presented as mean ± s.e.m (bar graph) from at least 3 independent biological replicates. Each biological replicate is depicted by a circle. *=p < 0.05, **=p < 0.01, ***=p < 0.001, ****=p < 0.0001.

SI Table 1. Control hiPSC NPC lines.

ID	Source	Patient ID	Source Cell	Reprogramming method	NPC line	Sex	Dx	Ethnicity	Age at Biopsy	IQ
C1	NIMH	NSB553	Fibroblast	SV-KOSM	NSB553 hiPSC#S1 NPC#1	M	Control	caucasian, non-Hispanic	31	127
C2	NIMH	NSB2607	Fibroblast	SV-KOSM	NSB2607 hiPSC#1 NPC#4	M	Control	caucasian, non-Hispanic	15	126
C3	NIMH	NSB690	Fibroblast	SV-KOSM	NSB690 hiPSC#2 NPC#1	M	Control	caucasian, non-Hispanic	25	115

SI Table 2. gRNA sequences.

gRNA Target	Oligo Sequence	
hKCTD13 gRNA #1	caccgGGAGCGCACGTCGACCCGCC	aaacGGCGGGTCGACGTGCGCTCCc
hKCTD13 gRNA #2	caccgGGTCGGCCGCATCCTCGATC	aaacGATCGAGGATGCGGCCGACCc
hKCTD13 gRNA #3	caccgAGCGCACGTCGACCCGCCCG	aaacCGGGCGGGTCGACGTGCGCTc
hTAOK2 gRNA #1	caccgGCGCAAAGATTCCTCGCACT	aaacAGTGCGAGGAATCTTTGCGCc
hTAOK2 gRNA #2	caccgGCGATCTGCGACTGCGCGCA	aaacTGCGCGCAGTCGCAGATCGCc
hTAOK2 gRNA #3	caccgGGCGATCTGCGACTGCGCGC	aaacGCGCGCAGTCGCAGATCGCCc
hNRXN1 gRNA #1	caccgCGTAGCCTACTGAGCATGCC	aaacGGCATGCTCAGTAGGCTACGc
hNRXN1 gRNA #2	caccgAGGAGTCGATAATTATGATG	aaacCATCATAATTATCGACTCCTc
hNRXN1 gRNA #3	caccgGCTCGGAACCCTTGAAAAGA	aaacTCTTTTCAAGGGTTCCGAGCCc
hNRXN1 gRNA #4	caccgCCGGGGCCGACAGGGTCAAAATG	aaacCATTTTGACCCTGTCGGCCCCGGc
hNRXN1 gRNA #5	caccgCAGTGGTACAGGGTAGCCACAGA	aaacTCTGTGGCTACCCTGTACCACTGc
hNRXN1 gRNA #6	caccgCCAGAGCCTGAAGCATGCATCGG	aaacCCGATGCATGCTTCAGGCTCTGGc
hSNAP91 gRNA #1	caccgGCGCGACGACGCCCTTGCCT	aaacAGGCAAGGGCGTCGTCGCGCc
hSNAP91 gRNA #2	caccgGACGGTCGCGGATGGCCGGC	aaacGCCGGCCATCCGCGACCGTCc
hSNAP91 gRNA #3	caccgGTTGGCCAAGACGGGCGAGT	aaacACTCGCCCGTCTTGGCCAACc
hCLCN3 gRNA #1	caccgGAGTAGCGTCGGCGCCTATT	aaacAATAGGCGCCGACGCTACTCc
hCLCN3 gRNA #2	caccgCGCCGACGCTACTCAGCGAG	aaacCTCGCTGAGTAGCGTCGGCGc
hCLCN3 gRNA #3	caccgGTGAGCTAATCGCTAATGAC	aaacGTCATTAGCGATTAGCTCACc
IVT *SNAP91* gRNA#3	TAATACGACTCACTATAGTTGGCCAAGACGGGCG	TTCTAGCTCTAAAACACTCGCCCGTCTTGGCCAA
IVT *FUT9* gRNA #1	TAATACGACTCACTATAGTACACGCGCGAGATCCAG	TTCTAGCTCTAAAACCTGGATCTCGCGCGTGTA
IVT *FUT9* gRNA #2	TAATACGACTCACTATAGACACGCGCGAGATCCAGA	TTCTAGCTCTAAAACTCTGGATCTCGCGCGTGT
IVT *FUT9* gRNA #3	TAATACGACTCACTATAGATGTTATGCATTACACCA	TTCTAGCTCTAAAACTGGTGTAATGCATAACAT
IVT *FUT9* gRNA #4	TAATACGACTCACTATAGCCAGATATTGGTTAGCAA	TTCTAGCTCTAAAACTTGCTAACCAATATCTGG
IVT *FUT9* gRNA #5	TAATACGACTCACTATAGATCCATTGTTGTAACCAG	TTCTAGCTCTAAAACCTGGTTACAACAATGGAT
IVT *FUT9* gRNA #6	TAATACGACTCACTATAGATTACTTGATGGGCTGGG	TTCTAGCTCTAAAACCCCAGCCCATCAAGTAAT
IVT *FUT9* gRNA #7	TAATACGACTCACTATAGGGGTATAGCTGCAAAAGG	TTCTAGCTCTAAAACCCTTTTGCAGCTATACCC
IVT *FUT9* gRNA #8	TAATACGACTCACTATAGGCTGGGGATGTAAGCTGG	TTCTAGCTCTAAAACCCAGCTTACATCCCCAGC
IVT *FUT9* gRNA #9	TAATACGACTCACTATAGGGTAATTGGGGATAGACA	TTCTAGCTCTAAAACTGTCTATCCCCAATTACC
IVT *FUT9* gRNA #10	TAATACGACTCACTATAGACAGTGGGTGAATTTGCA	TTCTAGCTCTAAAACTGCAAATTCACCCACTGT

IVT *CEP162* gRNA #1	TAATACGACTCACTATAGCAGATCATTTCAACCACT	TTCTAGCTCTAAAACAGTGGTTGAAATGATCTG
IVT *CEP162* gRNA #2	TAATACGACTCACTATAGGTGAAAACCCTTGAGGGG	TTCTAGCTCTAAAACCCCCTCAAGGGTTTTCAC
IVT *CEP162* gRNA #3	TAATACGACTCACTATAGAGATTGGCAAGTAAGGTG	TTCTAGCTCTAAAACCACCTTACTTGCCAATCT
IVT *CEP162* gRNA #4	TAATACGACTCACTATAGAAAGGTCTGACAAAAGGG	TTCTAGCTCTAAAACCCCTTTTGTCAGACCTTT
IVT *CEP162* gRNA #5	TAATACGACTCACTATAGAGACAGTGAAAACCCTTG	TTCTAGCTCTAAAACCAAGGGTTTTCACTGTCT
IVT *CEP162* gRNA #6	TAATACGACTCACTATAGACAGTGAAAACCCTTGAG	TTCTAGCTCTAAAACCTCAAGGGTTTTCACTGT
Negative Control (NC) gRNAs		
IVT *FUT9* NC gRNA #1	TAATACGACTCACTATAGTCTCCCAAATAGTATCTG	TTCTAGCTCTAAAACCAGATACTATTTGGGAGA
IVT *FUT9* NC gRNA #2	TAATACGACTCACTATAGATGCCACTCATCCAAACC	TTCTAGCTCTAAAACGGTTTGGATGAGTGGCAT
IVT *FUT9* NC gRNA #3	TAATACGACTCACTATAGGAGTGCAACATGACCAAG	TTCTAGCTCTAAAACCTTGGTCATGTTGCACTC
IVT *FUT9* NC gRNA #4	TAATACGACTCACTATAGGAGTGGCATCAGTATCAG	TTCTAGCTCTAAAACCTGATACTGATGCCACTC
IVT *FUT9* NC gRNA #5	TAATACGACTCACTATAGAACAAAGACATTGACCCA	TTCTAGCTCTAAAACTGGGTCAATGTCTTTGTT
IVT *FUT9* NC gRNA #6	TAATACGACTCACTATAGTACTGCTCTGTACCATGA	TTCTAGCTCTAAAACTCATGGTACAGAGCAGTA
IVT *FUT9* NC gRNA #7	TAATACGACTCACTATAGCCAACCACCACTTCAGCA	TTCTAGCTCTAAAACTGCTGAAGTGGTGGTTGG
IVT *FUT9* NC gRNA #8	TAATACGACTCACTATAGatATCTATGCCAAGATGG	TTCTAGCTCTAAAACCCATCTTGGCATAGATAT
IVT *FUT9* NC gRNA #9	TAATACGACTCACTATAGAACCACTTCAGCAGGGAGT	TTCTAGCTCTAAAACACTCCCTGCTGAAGTGGT
IVT *FUT9* NC gRNA #10	TAATACGACTCACTATAGTGGAAATATTTACCAAGG	TTCTAGCTCTAAAACCCTTGGTAAATATTTCCA
IVT *CEP162* NC gRNA #1	TAATACGACTCACTATAGGGGAAGAAGCGATCAGGG	TTCTAGCTCTAAAACCCCTGATCGCTTCTTCCC
IVT *CEP162* NC gRNA #2	TAATACGACTCACTATAGCCACCACCACTTACCCAA	TTCTAGCTCTAAAACTTGGGTAAGTGGTGGTGG
IVT *CEP162* NC gRNA #3	TAATACGACTCACTATAGAAGATAGAACCCAGCTGA	TTCTAGCTCTAAAACTCAGCTGGGTTCTATCTT
IVT *CEP162* NC gRNA #4	TAATACGACTCACTATAGAAAGGGATTAGCCTTAGG	TTCTAGCTCTAAAACCCTAAGGCTAATCCCTTT
IVT *CEP162* NC gRNA #5	TAATACGACTCACTATAGCAAGATAGAACCCAGCTG	TTCTAGCTCTAAAACCAGCTGGGTTCTATCTTG
IVT *CEP162* NC gRNA #6	TAATACGACTCACTATAGACAATAAAGGACGACCAA	TTCTAGCTCTAAAACTTGGTCGTCCTTTATTGT
IVT *CEP162* NC gRNA #7	TAATACGACTCACTATAGCATGGAAGTCCCTCAGCT	TTCTAGCTCTAAAACAGCTGAGGGACTTCCATG
IVT *CEP162* NC gRNA #8	TAATACGACTCACTATAGGGAAGAAGCGATCAGGGA	TTCTAGCTCTAAAACTCCCTGATCGCTTCTTCC
IVT *CEP162* NC gRNA #9	TAATACGACTCACTATAGTAGACTTTGCACACTGTG	TTCTAGCTCTAAAACCACAGTGTGCAAAGTCTA
IVT CEP162 NC gRNA #10	TAATACGACTCACTATAGACAGAAGTCCTACATACC	TTCTAGCTCTAAAACGGTATGTAGGACTTCTGT

SI Table 3. qPCR primer sequences.

mRNA Target	Oligo Sequence	
	Forward	**Reverse**
GAPDH	AGGGCTGCTTTTAACTCTGGT	CCCCACTTGATTTTGGAGGGA
B-ACTIN	TGTCCCCCAACTTGAGATGT	TGTGCACTTTTATTCAACTGGTC
KCTD13	TAACAGGACACCTGCAAACG	CTGGATGATGCCATGTCTTG
TAOK2	AGTCTAGCTCTTCTCCCCGC	CCGCCAAGCCCGAGTG
NRXN1	AGAAAGATGCCAAGCACCCA	CCCATGTCCAGGAGGAGGTA
SNAP91	AGGACCCATTAGCGGATCTTAACA	GCTCCCTTTGAAACTCAGCATCAA
CLCN3	AATCATAGGTCAAGCAGAGGGTCC	CCACAGGCATATGGAGCAAATACC
CEP162	TGCCTTGGTGGATAACTGAA	GAGAGAGGTTCCACTGCTCTT
FUT-9	TGTCTACGTGCTTCCCATGA	AACAGCCCAGGATAATGCAG
IVT SNAP91 #3	TTGGCCAAGACGGGCGAGT	CGACTCGGTGCCACTTTTTC

SI Table 4. Antibodies.

Antibody	Species	Supplier	Product Number	Dilution
GFAP	Ck	Aves Lab	GFAP	1:1000
EAAT1/GLAST	Rb	Boster Bio	PA2185	1:100
S100β	Ms	Sigma	S2532	1:1000
VIMENTIN	Rb	Cell Signaling	#3932	1:500
Cas9:AF-488	Ms	CST	34963S	5uL/1x10^6 cells

SUPPLEMENTAL EXPERIMENTAL PROCEDURES

hiPSC and NPC culture

All hiPSC and NPC lines were derived and validated as previously described; full details of the donors of the fibroblasts and validation of the hiPSC and NPC lines available (Topol et al., 2016) (**SI Table 1**). NPCs were maintained at high density, grown on growth factor reduced Matrigel (BD Biosciences) coated plates in NPC media (Dulbecco's Modified Eagle Medium/Ham's F12 Nutrient Mixture (ThermoFisher Scientific), 1x N2, 1x B27-RA (ThermoFisher Scientific) and 20 ng/ml FGF2 and split 1:3 every week with Accutase (Millipore, Billerica, MA, USA). Routine (every 4 weeks) mycoplasma testing was conducted using the MycoAlert Mycoplasma detection kit (Lonza); all cells used in this study were consistently negative.

Astrocyte differentiation

Antibiotic-selected dCas9-effector NPCs were differentiated to astrocytes and maintained as previously described (TCW et al., 2017). Astrocytes were cultured in astrocyte medium (ScienCell: 1801, astrocyte medium (1801-b), 2% fetal bovine serum (0010), astrocyte growth supplement (1852) and 10U/ml penicillin/streptomycin solution (0503) on Matrigel. Immunocytochemistry and FACS were used to validate NPC-astrocytes. Vendors, catalog numbers and dilutions of all antibodies used are listed in **SI Table 4**.

NGN2-induced neuronal differentiation

NGN2-induced neurons were derived from dCas9-effector NPCs as previously described (Ho et al., 2015) using the human *NGN2*-Neo lentiviral expressing vector (Addgene #79049). gRNA lentiviruses generated as above were co-transduced with induction viruses and cultures were spinfected (1 hour, 1000xg, 25°C). Cells were harvested at 9 days or 21 days later.

SUPPLEMENTAL REFERENCES

Brennand, K.J., Simone, A., Jou, J., Gelboin-Burkhart, C., Tran, N., Sangar, S., Li, Y., Mu, Y., Chen, G., Yu, D.*, et al.* (2011). Modelling schizophrenia using human induced pluripotent stem cells. Nature *473*, 221-225.

Ho, S.M., Hartley, B.J., Tcw, J., Beaumont, M., Stafford, K., Slesinger, P.A., and Brennand, K.J. (2015). Rapid Ngn2-induction of excitatory neurons from hiPSC-derived neural progenitor cells. Methods.

TCW, J., Wang, M., Pimenova, A.A., Bowles, K.R., Hartley, B.J., Lacin, E., Machlovi, S., Abdelaal, R., Karch, C.M., Phetnani, H.*, et al.* (2017). An efficient platform for astrocyte differentiation from human induced pluripotent stem cells. bioRxiv.

Topol, A., Zhu, S., Hartley, B.J., English, J., Hauberg, M.E., Tran, N., Rittenhouse, C.A., Simone, A., Ruderfer, D.M., Johnson, J.*, et al.* (2016). Dysregulation of miRNA-9 in a Subset of Schizophrenia Patient-Derived Neural Progenitor Cells. Cell reports *15*, 1024-1036.